1.0

1.1

1.25

2.8 2.5

4.5
5.0
5.6
6.3

3.2 2.2

3.6

4.0 2.0

1.8

1.4 1.6

MICROCOPY RESOLUTION TEST CHART
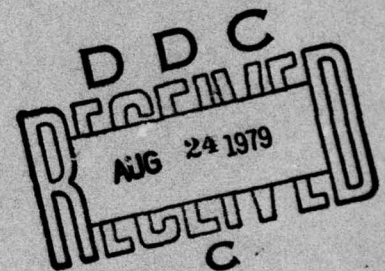NATIONAL BUREAU OF STANDARDS-1963-A

LEVEL

RASTER-SCAN DISPLAY PHOTOMETRIC NOISE MEASUREMENT

HARRY L. SNYDER, Ph.D
MAIER ALMAGOR, Ph.D.
DAVID I. SHEDIVY, M. S.

DEPARTMENT OF INDUSTRIAL ENGINEERING
  AND OPERATIONS RESEARCH
VIRGINIA POLYTECHNIC INSTITUTE & STATE UNIVERSITY
BLACKSBURG, VIRGINIA 24061

June 1979

D D C
RECEIVED
AUG 24 1979
C

79 08 23 036

NOTICES

When US Government drawings, specifications, or other data are used for any purpose other than a definitely related Government procurement operation, the Government thereby incurs no responsibility nor any obligation whatsoever, and the fact that the Government may have formulated, furnished, or in any way supplied the said drawings, specifications, or other data, is not to be regarded by implication or otherwise, as in any manner licensing the holder or any other person or corporation, or conveying any rights or permission to manufacture, use, or sell any patented invention that may in any way be related thereto.

Please do not request copies of this report from Aerospace Medical Research Laboratory. Additional copies may be purchased from:

> National Technical Information Service
> 5285 Port Royal Road
> Springfield, Virginia 22161

Federal Government agencies and their contractors registered with Defense Documentation Center should direct requests for copies of this report to:

> Defense Documentation Center
> Cameron Station
> Alexandria, Virginia 22314

TECHNICAL REVIEW AND APPROVAL

AMRL-TR-79-13

This report has been reviewed by the Information Office (OI) and is releasable to the National Technical Information Service (NTIS). At NTIS, it will be available to the general public, including foreign nations.

This technical report has been reviewed and is approved for publication.

FOR THE COMMANDER

CHARLES BATES, JR.
Chief
Human Engineering Division
Aerospace Medical Research Laboratory

REPORT DOCUMENTATION PAGE	READ INSTRUCTIONS BEFORE COMPLETING FORM

1. REPORT NUMBER	2. GOVT ACCESSION NO.	3. RECIPIENT'S CATALOG NUMBER
AMRL-TR-79-13		

4. TITLE (and Subtitle)	5. TYPE OF REPORT & PERIOD COVERED
RASTER-SCAN DISPLAY PHOTOMETRIC NOISE MEASUREMENT	Technical Report 08/75-12/77
	6. PERFORMING ORG. REPORT NUMBER YPI-HFL-79-1

7. AUTHOR(s)	8. CONTRACT OR GRANT NUMBER(s)
Harry L. Snyder, Ph.D. Maier Almagor, Ph.D. David I. Shedivy, M.S.	F33615-76-C-5022

9. PERFORMING ORGANIZATION NAME AND ADDRESS	10. PROGRAM ELEMENT, PROJECT, TASK AREA & WORK UNIT NUMBERS
Dept. of Industrial Engineering & Operations Res. Virginia Polytechnic Institute & State Univ. Blacksburg, VA 24061	62202F, 7184-11-05

11. CONTROLLING OFFICE NAME AND ADDRESS	12. REPORT DATE
Aerospace Medical Research Laboratory Aerospace Medical Division, AFSC Wright-Patterson AFB, OH 43433	June 1979
	13. NUMBER OF PAGES 70

14. MONITORING AGENCY NAME & ADDRESS(if different from Controlling Office)	15. SECURITY CLASS. (of this report)
	Unclassified
	15a. DECLASSIFICATION/DOWNGRADING SCHEDULE

16. DISTRIBUTION STATEMENT (of this Report)

Approved for public release; distribution unlimited.

17. DISTRIBUTION STATEMENT (of the abstract entered in Block 20, if different from Report)

18. SUPPLEMENTARY NOTES

19. KEY WORDS (Continue on reverse side if necessary and identify by block number)

Image quality
Television
Vision
Photometry

Displays
Noise

20. ABSTRACT (Continue on reverse side if necessary and identify by block number)

This report describes the results of two studies designed to measure dynamic noise, photometrically, on a raster-scan display. One study evaluated spot microphotometry of a single raster line; the other evaluated microdensitometric power spectral analysis of close-up photographs of raster lines.

The spot microphotometry technique proved superior and very reliable, yielding results that are highly correlated with input noise spectra.

DD FORM 1 JAN 73 1473

PREFACE

This study was initiated by the Visual Display Systems Branch, Human
Engineering Division of the Aerospace Medical Research Laboratory.
The research was conducted by the Department of Industrial Engineering
and Operations Research of Virginia Polytechnic Institute and State
University, Blacksburg, Virginia 24061, under Air Force Contract
F33615-76-C-5022. Dr. Harry L. Snyder was the principal investigator
for Virginia Polytechnic Institute and State University. Mr. Wayne L.
Martin and Dr. H. Lee Task were technical monitors for the Aerospace
Medical Research Laboratory.

This report covers research performed intermittently between August 1975
and December 1977, and serves as the final technical report for Task 2,
Photometric Noise Measurement.

Several persons have contributed substantially to the research described
in this report. Our thanks go to Charles D. Bernard and Willard W. Farley
for their equipment design and fabrication support; John E. Evans, III
for computer software support; Michael E. Maddox for the Fourier transform
analyses reported in Section V; and Eva D. McClain for manuscript prepara-
tion, administrative assistance, and other unsung but necessary duties.

1

TABLE OF CONTENTS

LIST OF TABLES

Table

LIST OF ILLUSTRATIONS

INTRODUCTION

Numerous laboratory and field investigations of raster-scan imaging
systems have demonstrated that the noise content of the displayed image
is a major contributor to the performance of the human observer in
obtaining information from the display. Theoretical and empirical
papers (e.g., Rosell and Willson, 1973; Snyder, 1973; Snyder, 1976;
Snyder, Keesee, Beamon, and Aschenbach, 1974) have all demonstrated
that various measures of object recognition and identification decrease
in quantity or quality as the video noise level increases relative to
the video signal.

Rosell and Willson (1973) have developed a systems-oriented theory to
predict performance as a function of SNR_D, the displayed signal-to-noise
ratio, based upon the assumption of an *ideal* kinescope, at least ideal
over the luminance and spatial frequency domains of pertinence to the
task and the observer. Other authors (e.g., Snyder *et al.*, 1974) have
questioned the appropriateness of this linearity assumption, and have
argued for the direct photometric measurement of displayed noise, rather
than the analytically derived value of SNR_D. (In the Rosell and Willson
concept, direct photometric measurement of signal and noise are not made,
nor is a measurement technique recommended.)

For this reason, Snyder *et al.* (1974) performed an initial evaluation of
a technique thought to measure photometrically root mean square noise at
the face of the display. In this technique, a small optical aperture was

6

focused on a raster scanning line (active portion only) and the RMS variability of this spot luminance, over a sample of 30 or so video frames, was recorded and analyzed. The correlation between this time-independent RMS luminance fluctuation (photometric noise) and the random input RMS electrical noise was evaluated for several combinations of line rate, video bandwidth, noise passband, and CRT luminance. The general results of this preliminary study are represented by figure 1, which shows a fairly linear relationship between RMS electrical (input) noise and RMS luminance (output noise) over the lower noise values, but an asymptotic output noise over a large portion of the input noise domain. The possible reasons for this nonlinear, asymptotic output relationship include (1) CRT luminance saturation, (2) inappropriate optical aperture size, (3) inappropriate optical aperture shape, or (4) nonindependent noise sampling of input random noise.
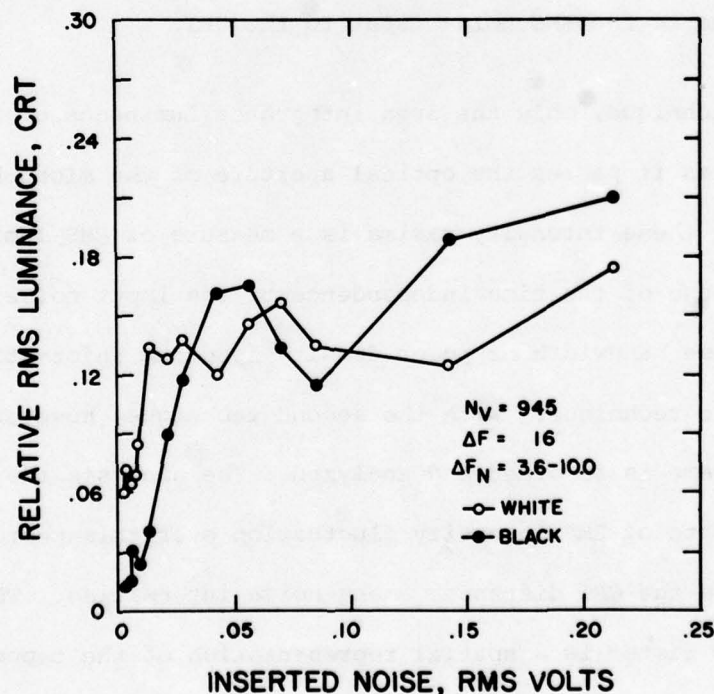
Figure 1. Example of Nonlinear Relationship Obtained between RMS Electrical Noise and RMS CRT Luminance, from Snyder *et al*. (1974)

7

One of the objectives of the research reported herein was to conduct a more thorough evaluation of this noise measurement technique, with parametric variation in (1) CRT luminance, (2) noise passband, (3) noise amplitude, and (4) optical aperture diameter.

The second objective of this research was to evaluate an alternate method of CRT photometric noise measurement. In this procedure, high resolution photographs are made of a single TV frame under known conditions of line rate, noise passband, and noise amplitude. The photographic transparencies are then scanned through a microdensitometer, with the scanning aperture centered on the film image of the active raster line. The output of the microdensitometer, as it scans the raster line image, is computer analyzed to obtain RMS density, or other related measures. Evaluation is then made of the relationship of this density spectrum to the RMS noise input to the CRT.

In the first technique, only the area integrated luminance of the CRT spot is sensed as it passes the optical aperture of the microphotometer. Variation among these intensity maxima is a measure of RMS luminance (or noise) because of the time independence of the input noise distribution. However, no noise bandwidth or power density spectrum information can be obtained by this technique. With the second technique, however, an area of the video frame is recorded and analyzed. The analysis thereby yields an estimate of RMS intensity fluctuation over this photographed area, as well as the CRT distances among noise intensities. That is, because the CRT raster is a spatial representation of the temporally random noise input signal, both (temporal) frequency and intensity estimates can be made from this photometric sample. Accordingly, the

8

second measurement technique permits estimation of the photometric

power density spectrum of the noise, which can be compared to the known

noise input power density spectrum.

Details of these two measurement techniques and their results are
described in the following sections. It should be noted that no human

observer performance data are presented in this report since the effects

of noise amplitude and noise passband upon observer performance have

been quantified elsewhere (e.g., Keesee, 1976; Rosell and Willson, 1973;

Snyder *et al.*, 1974). Rather, the emphasis is upon the suitability and

ease of implementation of these photometric noise measurement techniques.

<center>METHOD: CRT SPOT MICROPHOTOMETRY</center>

APPARATUS

Television System

The TV system used in this experiment is diagrammed in figure 2. A
COHU Model 7100 camera, a COHU Model 6900 camera control unit, and a
Conrac Model QQA monitor (43 cm diagonal) with a P4 phosphor comprised
the basic video chain, which was operated at 945 lines/frame with a
positive 2:1 interlace. Previous measurements indicated that the TV
system had an electronic bandwidth of over 30 MHz (-3 dB), but that some
equivalent bandwidth loss existed in the electron-photon conversion at
the CRT (Snyder, 1976). The "photometric bandwidth" is estimated to be
on the order of 18-20 MHz.
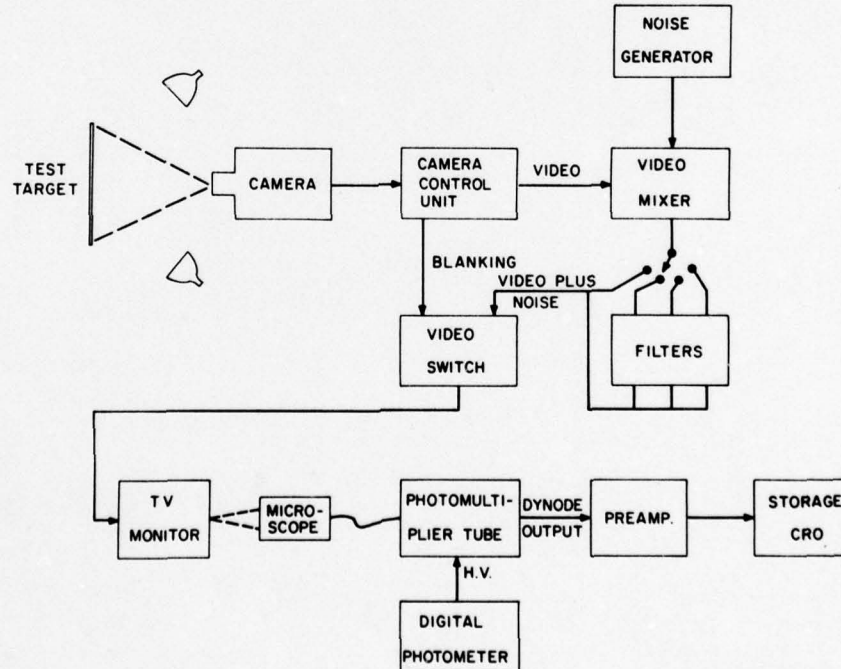
Figure 2. Equipment Block Diagram

<center>10</center>

The camera was mounted in a large dark box and focused upon a target area 20.3 × 25.4 cm which held various stiff cardboard targets. A gray scale target was located here for system setup and calibration, while a specially made target was used for experimental measurements. Targets were illuminated at 45 deg angles by two 150 W photofloods.

A custom-designed, wideband (40 MHz) video mixer combined the camera output video with the noise produced by a General Radio Model 1383 noise generator, whose output was random, Gaussian amplitude noise from 20 Hz to 20 MHz. A Tektronix Model 7L13 spectrum analyzer verified the noise spectrum.

As required by the experimental design, passive low-pass filters were used to reduce the passband of video and noise. These filters had -3 dB down points of 10, 5, and 2.5 MHz, with rolloffs of -6 dB per octave. They were inserted in the video chain after the video mixer (figure 2).

During both horizontal retrace and vertical flyback, the video was blanked by a custom designed switch to prevent shifts in the DC video level, either between lines or between frames, caused by random noise fluctuations. Without such noise blanking, spurious noise-coupled luminance changes might result.

Noise amplitude was set by an output potentiometer on the noise generator and monitored, at the CRT input, by a Ballantine Model 323-01 True RMS Voltmeter. The passive low-pass filters were removed from the circuit when noise measurements were made; i.e., RMS noise values are for the 20 Hz to 20 MHz noise generator output into the CRT, without attenuation by the low-pass filters.

11

Photometric Measurement

A Gamma Scientific Model 2400 digital photometer was used for noise measurement. The photometric microscope of this system can accept various apertures and objective lenses which, in combination, produce numerous effective aperture sizes in the object plane. For this experiment, five object-plane aperture sizes were used, as indicated in table 1.

Table 1. OBJECT-PLANE CIRCULAR EFFECTIVE APERTURE DIAMETERS, AS DETER-
MINED BY COMBINATIONS OF OBJECTIVE LENS AND EYEPIECE APERTURE

Field Aperture Diameter	Objective Lens Magnification Factor		
	1X	2.5X	4X
150 μ		60 μ	37.5 μ
450 μ	450 μ	180 μ	112.5 μ

The photometric microscope was mounted on a vernier-controlled X-Y stage which permitted accurate centering of the object-plane aperture on an active raster line in the approximate center of the display. The radiant energy collected by the microscope eyepiece was transmitted to the photomultiplier tube by a fiber-optics bundle. This energy was then filtered by a photomultiplier-matched photopic sensitivity function filter to produce an input to the digital photometer in proportion to photopic luminance of the CRT spot.

Because the output of the digital photometer is integrated, over time, for each analog-to-digital conversion (minimum time constant is 0.01 s), it was necessary to bypass this conversion to sample the higher frequency

12

flying spot on the CRT. Thus, a wideband preamplifier was designed to
take the output directly from the dynode of the photomultiplier tube
and provide a wideband (20 MHz), high impedence signal for display on
a cathode-ray oscilloscope. This preamplifier output from the photo-
multiplier was calibrated by having the photometric microscope focused
on a standard Gamma Scientific 342.6 cd/m^2 luminance source. The dynode
output was displayed on a Tektronix Model 7623 storage socilloscope with
the time base adjusted to sweep the oscilloscope display every second,
thereby providing at least 25 samples of spot luminance on the stored
oscilloscope display. The maximum values of these 25 samples ("spikes")
represent the calibrated luminances of the CRT spot on 25 successive
frames. Fluctuations among these calibrated luminance values can be
converted to RMS luminance.

EXPERIMENTAL DESIGN

The experimental design was a four-variable factorial, consisting of
(1) three target luminances (10.63, 17.32, and 36.11 cd/m^2); (2) four
noise passbands (20 Hz - 20 MHz, 20 Hz - 10 MHz, 20 Hz - 5 MHz, and
20 Hz - 2.5 MHz); (3) five object-plane sampling apertures (37.5, 60,
112.5, 180, and 450 μ); and (4) six noise amplitudes (0, 40, 80, 120,
160, and 200 mV, RMS). Fifty samples (or two stored and measured
oscilloscope display frames) were obtained for each of the 3 × 4 × 5
× 6 = 360 experimental conditions, for a total data set of 18,000 samples.

PROCEDURE

The experiment was conducted over a 5-day period, with all measurements
for a given sampling aperture being made on a single day. On each day,
the TV and photometer systems were turned on 45 min prior to data

13

collection to assure temperature stabilization. Following this warm-up period, the amplitude of the video signal from the camera control unit was adjusted to a total of 640 mV, peak-to-peak, with 280 mV of peak-to-peak video signal riding 360 mV above the sync tip. The test target for this procedure was a 20.3 by 25.4 cm, 10-step gray scale, in the center of which were three test luminance patches, each approximately 1 cm square. The monitor brightness and contrast controls were then adjusted to produce specific luminance values for each of the 10 gray steps, ranging from 1.0 to 36.11 cd/m^2. These luminance values at the CRT were linearly related to the reflectances of the gray steps on the target, thus assuring a linear luminance response over this range. When the video system was calibrated, the three small luminance test patches in the center had displayed luminances of 10.63, 17.32, and 36.11 cd/m^2. They were equivalent to steps 3, 4, and 10 on the gray scale target, respectively.

The correct combination of objective lens and microscope field aperture was then affixed to the microscope, and the photometer output on the storage oscilloscope was calibrated to the 342.6 cd/m^2 source.

The experimenter then focused the microscope on an active raster line at the approximate center of the selected test luminance patch. With the oscilloscope in the nonstorage mode, and the output of the photo-multiplier tube indicated on the oscilloscope, the experimenter adjusted the vertical vernier control of the microscope stand to maximize the signal. In this manner, the sampling aperture was centered on an active raster line. With the time base of the oscilloscope set at 0.1 s per major division, the experimenter engaged the single shot storage mode,

14

thereby "freezing" a sample of 25 to 30 spot amplitudes, one per TV frame. The first 25 peak amplitudes were manually recorded, and two such 25-sample recordings were made for each experimental combination. After the three test luminance patches were measured without filter or noise, filter or noise levels were changed, and all test luminance patches were measured again. All combinations of 4 filters × 6 noise levels × 3 luminances were measured each day. Periodic checks of the camera, camera control unit, and monitor voltage/luminance levels were made to assure system stability and lack of discernible drift.

RESULTS: CRT SPOT MICROPHOTOMETRY

The 50 luminance values per experimental condition were used to obtain
a mean and standard deviation (RMS luminance). Analyses of variance
were then performed on both mean luminance and RMS luminance measures.

MEAN LUMINANCE

Table 2 summarizes the analysis of variance of mean luminance. Nearly
all main effects and interactions are highly significant statistically.
Figure 3 illustrates the Test Luminance main effect, which merely veri-
fies that the overall luminance of the test patch is accurately
measured by the mean amplitude of the individual spot samples. Any
deviation from linearity would be an indication of nonlinearity or
inaccuracy in the measurement technique. As seen in figure 3, the
results are extremely accurate and serve to support the validity of
the measurement approach.

Figure 4 illustrates the effect of noise bandwidth on mean displayed
luminance. Since the noise is AC coupled, there should not be any noise
bandwidth effect on *mean* luminance (but there should be, of course, on
RMS luminance). This effect, though statistically significant, is of
little practical importance, and is probably due to very small filter
insertion losses.

Figure 5 illustrates the main effect of the sampling aperture diameter
upon measured mean luminance. While the mean for the 112.5 μ aperture
appears unduly high, the general trend is clear. As the aperture size

16
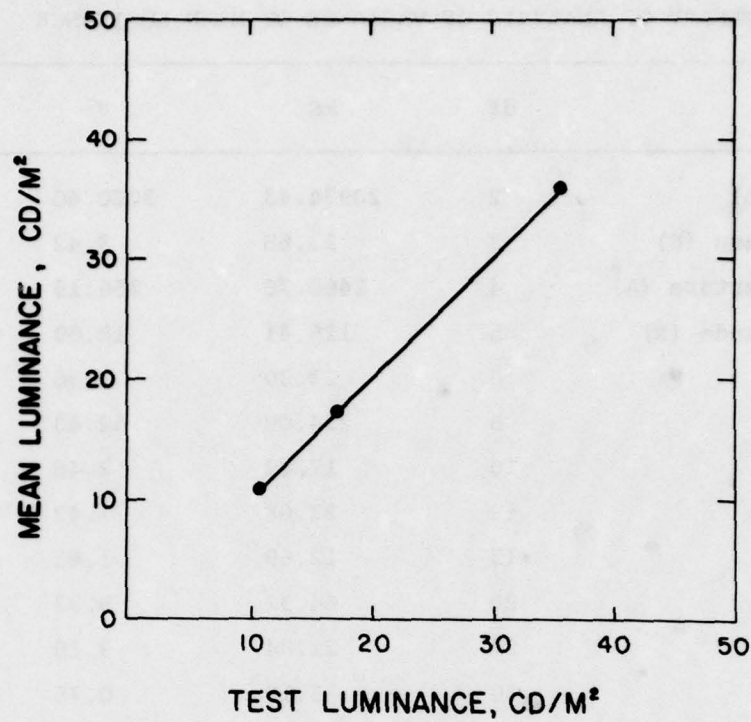
Figure 3. Effect of Test Luminance on Measured Mean Luminance
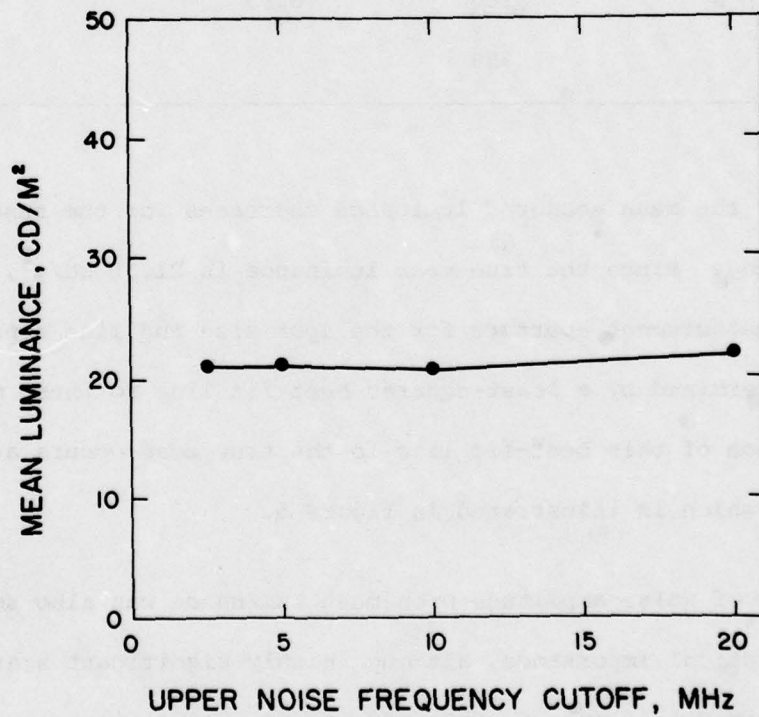
Figure 4. Effect of Noise Bandpass on Measured Mean Luminance

17

Table 2. SUMMARY OF ANALYSIS OF VARIANCE OF MEAN LUMINANCE

Source	df	MS	F	p
Luminance (L)	2	20934.43	3020.40	0.0001
Noise Bandpass (F)	3	23.68	3.42	0.0195
Sampling Aperture (A)	4	2468.76	356.19	0.0001
Noise Amplitude (N)	5	125.41	18.09	0.0001
L × F	6	23.30	3.36	0.0043
L × A	8	294.09	42.43	0.0001
L × N	10	17.22	2.48	0.0096
F × A	12	23.68	3.42	0.0003
F × N	15	12.69	1.83	0.0375
A × N	20	64.92	9.37	0.0001
L × F × A	24	21.84	3.15	0.0001
L × F × N	30	5.19	0.75	> 0.05
L × A × N	40	16.40	2.37	0.0002
F × A × N	60	6.02	0.87	> 0.05
L × F × A × N	120	6.93		
Total	359			

increases, the mean measured luminance decreases for the range of apertures investigated. Since the true mean luminance is 21.35 cd/m^2, the most accurate measurement aperture for the spot size and line separation used can be determined by a least-squares best-fit line to these means. The intersection of this best-fit line to the true mean occurs at an aperture of 168 μ, which is illustrated in figure 5.

The effect of Noise Amplitude upon mean luminance was also small and of little practical importance, although highly significant statistically. As illustrated in figure 6, this effect was inconsistent and probably is a spurious one due to slightly inconsistent output from either the noise

18
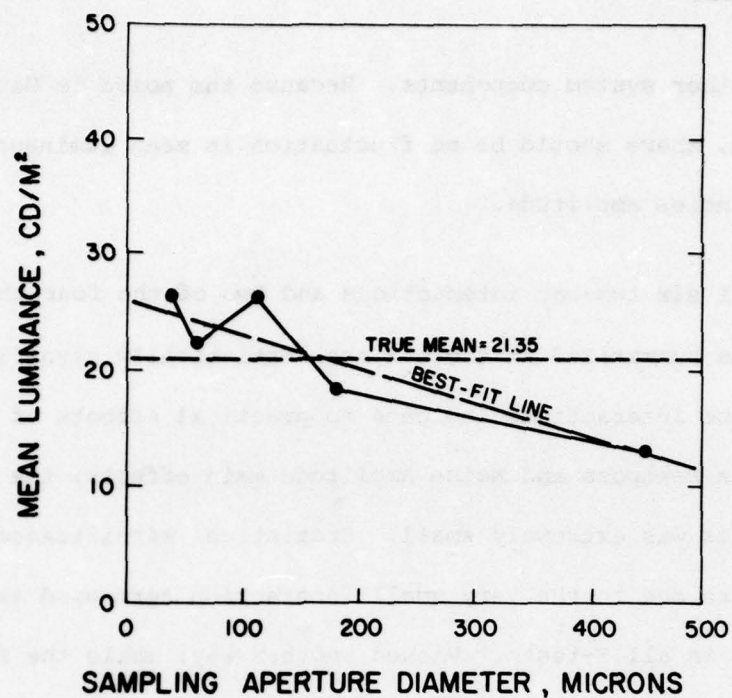
Figure 5. Effect of Sampling Aperture Size on Measured Mean Luminance
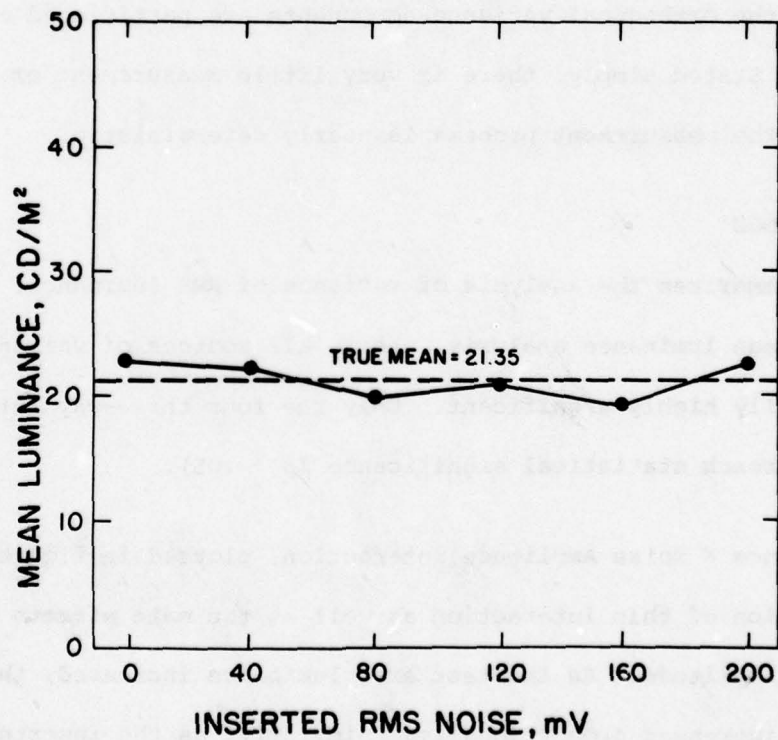
Figure 6. Effect of Noise Amplitude on Measured Mean Luminance

source or other system components. Because the noise is Gaussian with a zero mean, there should be no fluctuation in mean luminance with changes in noise amplitude.

Although all six two-way interactions and two of the four three-way interactions summarized in table 2 are statistically significant, plots of each of these interactions indicate no practical effects of interest. As in the Noise Bandpass and Noise Amplitude main effects, the magnitude of these effects was extremely small. Statistical significance in these cases appears due to the very small interaction term used as the denominator in all F-tests. Viewed another way, while the F-tests are all statistically conservative, as estimated by an expected mean square analysis, the random fluctuation among cells is very small, and essentially zero once the orthogonal variance components are partitioned out in the analysis. Stated simply, there is very little measurement or experimental error, as the measurement process is nearly deterministic.

RMS LUMINANCE

Table 3 summarizes the analysis of variance of RMS luminance. Again, as with the mean luminance analysis, nearly all sources of variance were statistically highly significant. Only the four three-way interactions failed to reach statistical significance ($p > .05$).

The Luminance × Noise Amplitude interaction, plotted in figure 7, permits visualization of this interaction as well as the main effects of Luminance and Noise Amplitude. As the test area luminance increased, the RMS luminance increased proportionally. Similarly, as the inserted electrical noise increased, the output photometric noise increased, with a suggested

20

Table 3. SUMMARY OF ANALYSIS OF VARIANCE OF RMS LUMINANCE

Source	df	MS	F	p
Luminance (L)	2	353.91	274.75	0.0001
Noise Bandpass (F)	3	120.64	93.66	0.0001
Sampling Aperture (A)	4	153.71	119.32	0.0001
Noise Amplitude (N)	5	145.00	112.56	0.0001
L × F	6	4.16	3.23	0.0056
L × A	8	14.02	10.89	0.0001
L × N	10	16.58	12.87	0.0001
F × A	12	4.66	3.62	0.0001
F × N	15	13.83	10.74	0.0001
A × N	20	3.74	2.91	0.0002
L × F × A	24	1.10	0.86	> 0.05
L × F × N	30	1.60	1.24	> 0.05
L × A × N	40	1.74	1.35	> 0.05
F × A × N	60	1.22	0.87	> 0.05
L × F × A × N	120	1.29		
Total	359			

trend for the output noise to increase in an accelerating manner. That is,
the slope of the output noise function appears to increase with greater
input noise levels. Statistical analyses, however, result in a rejection
($p > .05$) of a significant curvilinear relationship for the three
Luminance levels; the least-squares, best-fit straight lines, for the
three Luminance levels in increasing order are:

$$\text{RMS cd/m}^2 = 2.700 + 0.0111 \text{ RMS mV};\tag{1}$$

$$\text{RMS cd/m}^2 = 3.134 + 0.0170 \text{ RMS mV; and}\tag{2}$$

$$\text{RMS cd/m}^2 = 3.870 + 0.0330 \text{ RMS mV.}\tag{3}$$
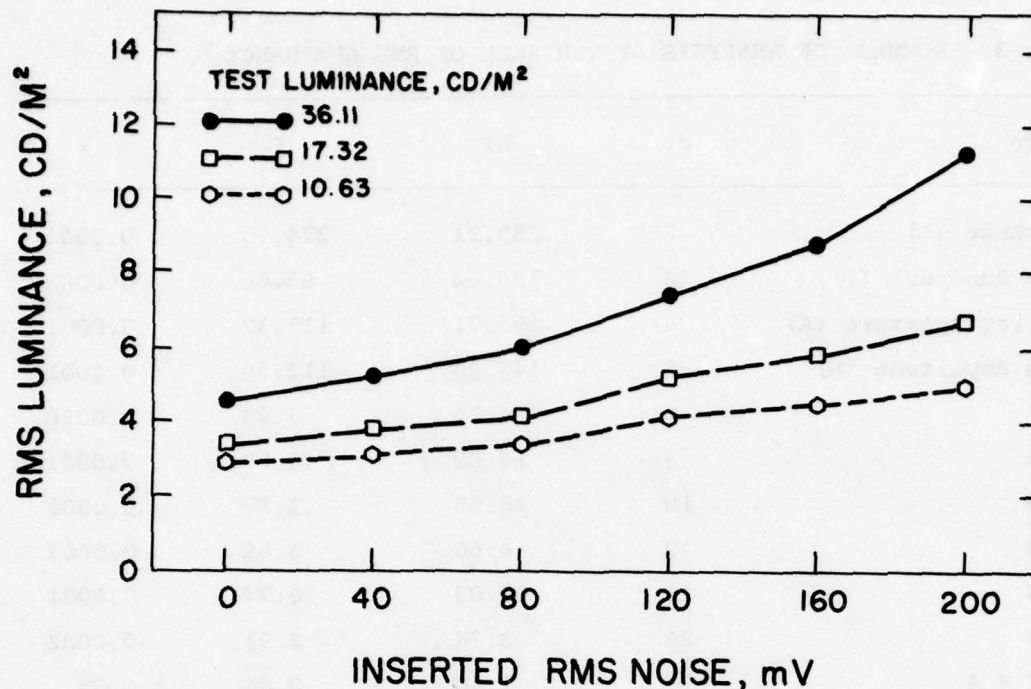
Figure 7. Effect of Test Luminance × Noise Amplitude Interaction on RMS Luminance

The coefficients of determination, r^2, for the three Luminances, also in increasing order, are 0.976, 0.980, and 0.958, respectively. All are statistically significant ($p < .0001$). Collapsing across all three Test Luminance levels, the least-squares best-fit line relating luminance noise to inserted electrical noise is:

RMS cd/m^2 = 3.258 + 0.0205 RMS mV .   (4)

The coefficient of determination for this main effect is $r^2 = 0.976$, $p < .0001$.

It should be noted in figure 7 that the zero input noise level results in some measurable photometric noise, ranging from 2.70 to 3.87 cd/m^2, depending upon the Test Luminance level. The present data do not permit

22

determination of whether this zero input photometric noise is due to inherent noise in the photometer, or to display-related noise (e.g., phosphor noise). Since the photometric noise does vary with input luminance, at least some of this measured noise is likely to be display related, for photometer noise should be essentially constant.

The Noise Amplitude × Noise Bandpass interaction is illustrated in figure 8. Again, the effects of both Noise Amplitude and Noise Bandpass on RMS luminance are essentially linear, with a slight increase in slope for increases in Noise Bandpass. The least-squares, best-fit lines relating RMS luminance to inserted noise, for the four Noise Bandpasses (indicated as subscripts), are:

$$RMS_{2.5} \; cd/m^2 = 3.607 + 0.002 \; RMS \; mV; \tag{5}$$

$$RMS_5 \quad cd/m^2 = 3.048 + 0.018 \; RMS \; mV; \tag{6}$$

$$RMS_{10} \quad cd/m^2 = 2.896 + 0.024 \; RMS \; mV; \text{ and} \tag{7}$$

$$RMS_{20} \quad cd/m^2 = 3.488 + 0.034 \; RMS \; mV. \tag{8}$$

The slopes of the best-fit lines increase consistently with increases in Noise Bandpass. The coefficients of determination for these four sets of data, respectively, are 0.886, 0.921, 0.914, and 0.982 (all $p < .001$).

It should be expected that RMS luminance increases as Noise Bandpass increases because of the manner by which the inserted noise was measured. Specifically, the inserted noise was measured in the absence of any bandwidth limiting filters; thus, noise power into the CRT decreased as the noise passband was attenuated by the low-pass filters. Table 4 gives the actual RMS noise into the TV monitor preamplifier for each of the noise level/filter combinations.
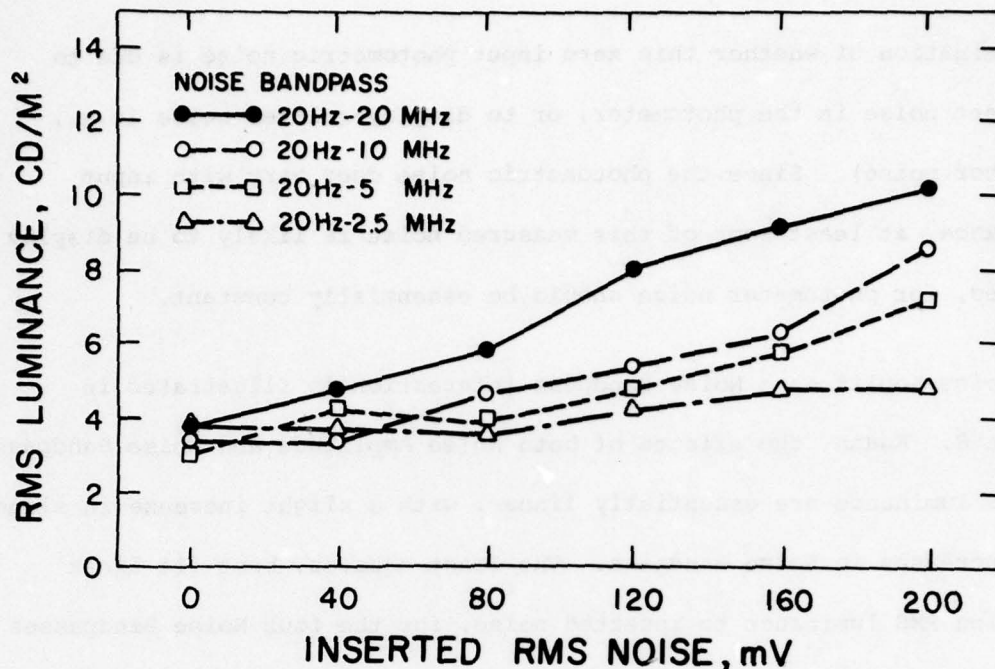
Figure 8. Effect of Noise Bandpass × Noise Amplitude Interaction on RMS Luminance

These tabled values, plus the nominal Noise Amplitude values for the 20 Hz - 20 MHz Noise Passband, should be expected to correlate highly with the measured RMS luminance. This coefficient of determination, r^2, is 0.891, and the least-squares, best-fit linear relationship is:

$$\text{RMS cd/m}^2 = 2.816 + 0.035 \text{ RMS mV}_{\text{CRT}} \text{ .}$$ (9)

Thus, if the true RMS noise delivered to the monitor is known, equation (9) can be used to predict 89% of the RMS luminance noise at the CRT. If, on the other hand, either bandpass filters are inserted to limit noise, or the video monitor has a known, restricted bandpass, equations (5) through (8) can be used to predict RMS luminance noise, with prediction ranging from 89% to 98%. In either case, the displayed noise is accurately predicted from knowledge of the input noise. (It should be

24

Table 4. POST-FILTER INSERTED RMS NOISE, mV

Pre-Filter Noise, RMS mV	Filter Passband		
	20 Hz - 10 MHz	20 Hz - 5 MHz	20 Hz - 2.5 MHz
0	0.0	0	0.0
40	28.3	20	14.1
80	56.6	40	28.3
120	84.8	60	42.4
160	113.1	80	56.6
200	141.4	100	70.7

noted that the measurement of input noise without any bandpass filters was deliberate, based upon the assumption that typical low light level or photon noise limited systems have a predictable or measurable *input* noise which can be filtered at the display input. Thus, the more meaningful systems measurement of noise, in this context, is pre- and not post-filter. Values calculated in table 4 were empirically verified.)

Equation (9) can also be used to predict nonremovable displayed noise. Letting input noise equal zero, the predicted RMS luminance at the CRT is 2.816 cd/m^2, the random noise attributable to such sources as raster instability, power supply fluctuation, preamplifier generated noise, and a variety of other causes. Thus, a raster scan display will *always* have some amount of dynamic, uncorrelated noise, which probably accounts for the fact that the visual sine-wave threshold is higher for a raster-scan display than for other displays with zero noise input (Keesee, 1976).

Finally, figure 9 illustrates the effect of the Sampling Aperture × Noise Amplitude interaction on the measured RMS luminance. Again, RMS luminance increases linearly with inserted noise for each sampling

aperture, and the slope of these linear relationships generally decreases

with increases in the aperture size. Table 5 indicates the least-squares,

best-fit equations and the coefficients of determination for each of the

sampling apertures.
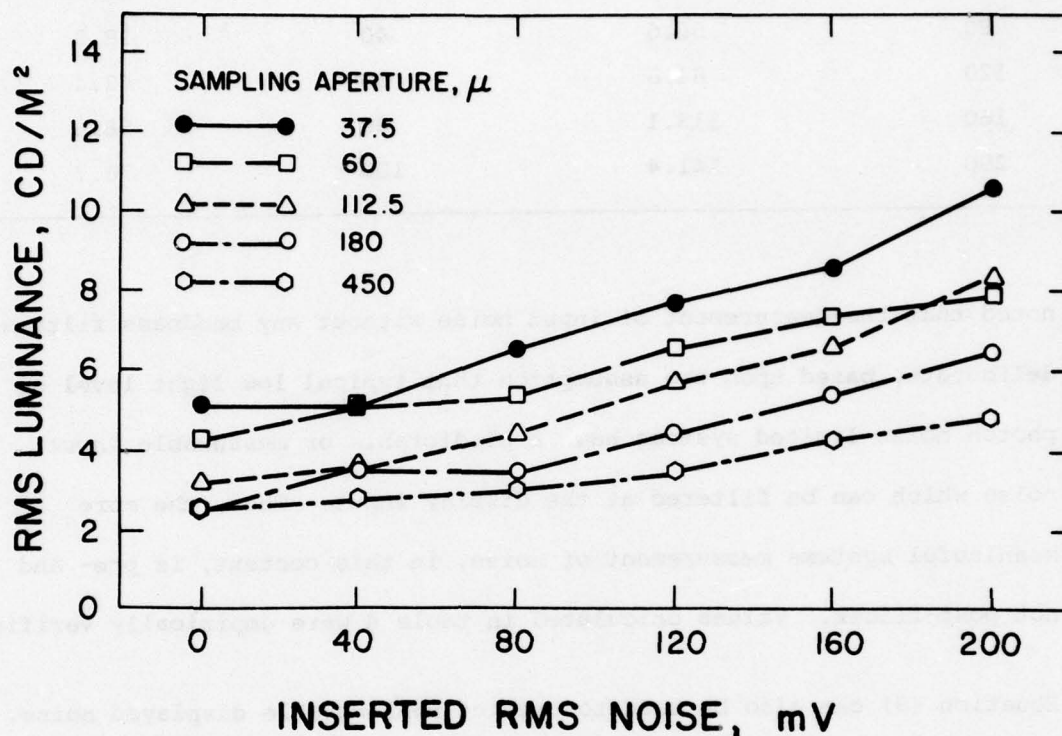
Figure 9. Effect of Sampling Aperture × Noise Amplitude Interaction
on RMS Luminance

For this particular line rate (945 lines/frame) and CRT size (43.2 cm

diagonal), the 112.5 micron aperture yields the best linear prediction,

$\sqrt{r^2}$ = 97% of the RMS luminance given the input RMS voltage. Other

aperture sizes resulted in predicted RMS luminance variance ranging upward

from 94%. Thus, all the aperture sizes evaluated in this experiment

produced excellent prediction from the known input noise voltage. These

aperture sizes ranged from 12.8% to 513.1% of the center-line to center-

line distance (0.294 mm) between adjacent raster lines.

26

Table 5. LEAST-SQUARES, BEST-FIT FUNCTIONS FOR FIVE SAMPLING APERTURES

Aperture, Microns	Best-Fit Equation				r^2
	RMS cd/m^2 = _____	+	_____	RMS mV	
37.5	4.451		0.028		0.946
60.0	4.327		0.016		0.946
112.5	2.763		0.026		0.974
180.0	2.526		0.018		0.937
450.0	2.352		0.012		0.945

SENSITIVITY ANALYSIS

While the above described overall relationships are orderly and satisfyingly accurate in prediction of RMS luminance, one needs to optimize the means by which photometric noise at the CRT is measured. For this reason, analyses were performed to determine those conditions leading to the greatest linearity, as indicated by a maximal r^2, and to the greatest sensitivity, as indicated by the greatest slope of the least-squares, best-fit line.

For each of the 5 (Sampling Apertures) × 4 (Noise Passbands) × 3 (Test Luminances) = 60 conditions, a least-squares best-fit line was calculated, predicting RMS luminance from inserted noise voltage. Slopes and r^2 values for each least-squares, best-fit line were calculated, and separate analyses of variance were performed using the slopes and r^2 values as dependent variables. Newman-Keuls multiple comparison tests were then applied to significant effects to determine those specific independent variable levels which resulted in greater linearity and slope.

Analysis of r^2

Table 6 summarizes the analysis of variance of r^2 scores. The only significant effects were Luminance and Noise Bandpass.

Table 6. SUMMARY OF ANALYSIS OF VARIANCE OF r^2 VALUES

Source	df	MS	F	p
Luminance (L)	2	0.1431	3.53	0.0454
Noise Bandpass (F)	3	0.9106	22.44	0.0001
Sampling Aperture (A)	4	0.0862	2.12	> 0.05
L × F	6	0.0025	0.06	> 0.05
L × A	8	0.0835	2.06	> 0.05
F × A	12	0.0415	1.02	> 0.05
L × F × A	24	0.0405		
Total	59			

The mean r^2 values for the three Luminance levels were 0.546 for 10.63 cd/m^2, 0.636 for 17.32 cd/m^2, and 0.716 for 36.11 cd/m^2. Each of the three mean r^2 values was significantly different ($p < .05$) from the other two using the Newman-Keuls test. Thus, the average linearity of regression increases consistently with increases in CRT luminance, and the most linear measures of RMS noise are made at the highest luminance level.

The largest mean value of r^2 was obtained for the 20 Hz to 20 MHz noise passband ($r^2 = 0.822$), with decreases in bandwidth yielding consistent decreases in r^2, 0.761 for 20 Hz - 10 MHz, 0.673 for 20 Hz - 5 MHz, and 0.275 for 20 Hz - 2.5 MHz. Newman-Keuls tests revealed that the r^2 value of 0.275 for 20 Hz - 2.5 MHz was significantly ($p < .01$) less than

28

any of the other three, and that the other three did not differ significantly among themselves.

Analysis of Slope

Table 7 summarizes the analysis of variance of the calculated slopes for the 60 combinations of L, F, and A. As shown, only the Noise Bandpass × Sampling Aperture interaction failed to reach statistical significance.

Table 7. ANALYSIS OF VARIANCE OF SLOPE VALUES

Source	df	MS	F	p
Luminance (L)	2	0.00264	61.10	0.0001
Noise Bandpass (F)	3	0.00213	49.35	0.0001
Sampling Aperture (A)	4	0.00052	11.96	0.0001
L × F	6	0.00015	3.61	0.0108
L × A	8	0.00012	2.86	0.0220
F × A	12	0.00005	1.15	> 0.05
L × F × A	24	0.00004		
Total	59			

Figure 10 illustrates the effect of the Luminance × Noise Bandpass interaction upon the mean slope. Increases in either Luminance or Noise Passband cause increasing slopes. Further analysis by the Newman-Keuls test added little useful information.

The mean slopes for the three Luminance levels (0.0111 for 10.63 cd/m^2, 0.0169 for 17.32 cd/m^2, and 0.0332 for 36.11 cd/m^2) all differ from one another (p < .01) by the Newman-Keuls test, as do the four means for the Noise Bandpass main effect levels (0.0050, 0.0182, 0.0238, and 0.0341,

29
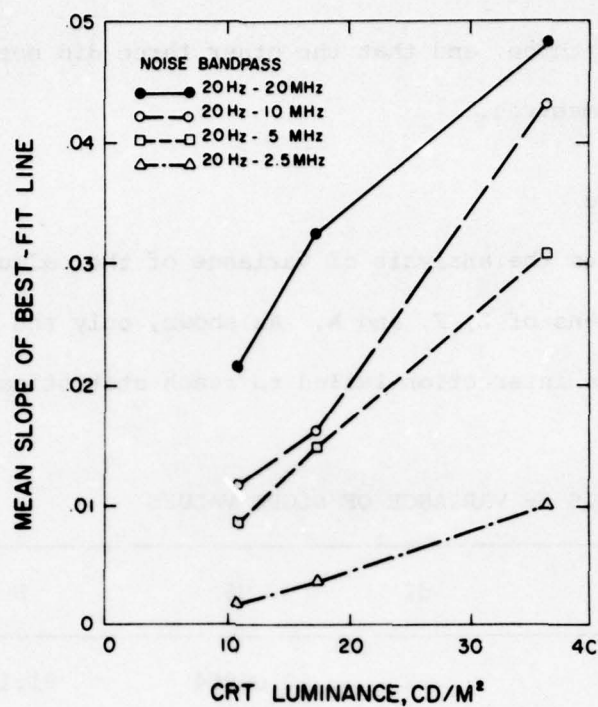
Figure 10. Effect of Luminance × Noise Bandpass Interaction on
Mean Slope
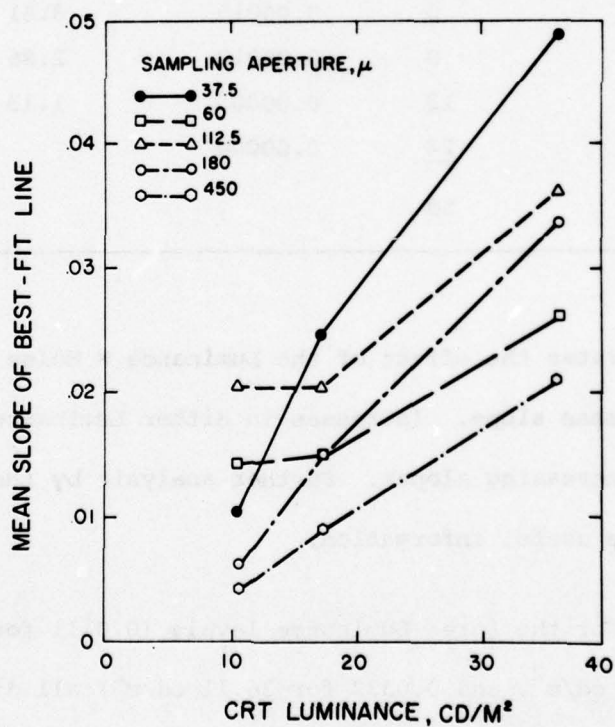
Figure 11. Effect of Luminance × Sampling Aperture Interaction on
Mean Slope

30

respectively). Thus, in general, the greater the CRT luminance or the wider the inserted noise passband, the more sensitive is the measurement of RMS luminance as indicated by the linear slope.

Figure 11 illustrates the Luminance × Sampling Aperture interaction. While the Luminance main effect was described above, it is important to note that the Sampling Aperture main effect is also significant ($p < .0001$), although probably not as important in noise measurement as is the interaction between the CRT luminance and the selected aperture.

As illustrated in figure 11, increases in mean slope are obtained with decreasing aperture size. The smallest aperture (37.5 µ) results in a greater mean slope (0.0280) than do aperture sizes of 60 µ, 180 µ, or 450 µ. The mean slope obtained for the 112.5 µ aperture size is not significantly ($p > .05$) different from that of the 37.5 µ aperture. Because the combination of the 37.5 µ aperture and the lowest (10.63 cd/m^2) luminance results in an unexpectedly poor mean slope, the 37.5 µ aperture should be avoided for low luminances, but it is clearly preferred for luminances above approximately 15 cd/m^2. This sampling aperture selection problem will be discussed further in the section dealing with film microdensitometry.

31

By this method, 35-mm photographs are taken of a small portion of the
TV frame at a scale which permits microdensitometric evaluation of the
individual raster line containing the inserted random noise. Care is
taken to select the photographic scale so as not to be measurement
limited by the photographic process. Because the film exposure time
is limited to one TV frame period, 1/30 s, no TV noise integration
occurs in the filming process.

The resulting 35 mm film frames are then analyzed by scanning a portion
of the length of each raster line image with a microdensitometer,
recording the density changes along the lines, which were caused by
the noise inserted into the video system. The noise power spectrum,
as measured on film, should closely reflect that inserted into the
video system if the film-microdensitometric scanning-analysis system
is linear. Any departure from linearity would of course reduce the
extent of this relationship and the resulting utility of the technique.

TV SYSTEM

The video system configuration used in this research is diagrammed in
figure 12. A specially designed control unit generated a 525-line,
2:1 positively interlaced raster, with the necessary sync and blanking
signals. A video switch was opened during the blanked interval, and
closed during the active video interval. In this manner, the inserted
noise from a General Radio Model 1383 noise generator was mixed with
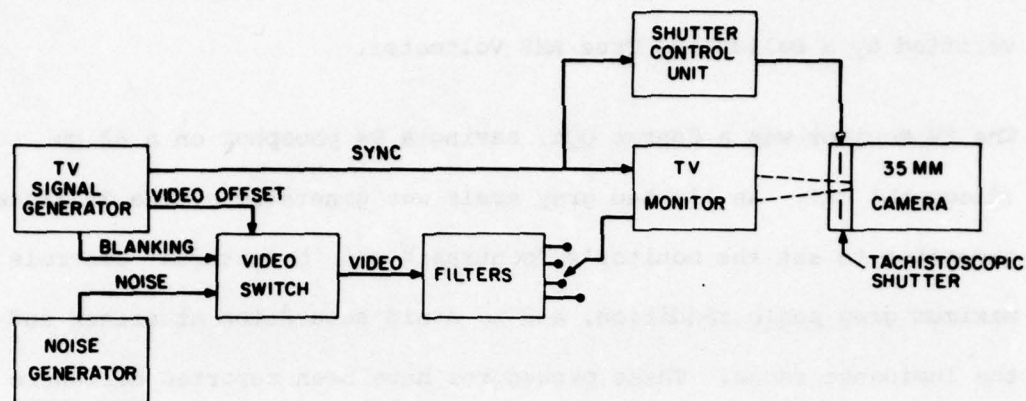
Figure 12. Equipment Block Diagram

the DC video level during the active video line, but not with the video
sync signals during retrace and flyback. Passive low-pass filters were
used to set the noise bandwidth at four levels: (1) 20 Hz - 20 MHz (no
filter); (2) 20 Hz - 10 MHz; (3) 20 Hz - 5 MHz; and (4) 20 Hz - 2.5 MHz.
Upper bandwidth values are -3 dB (voltage output), and the filter
rolloff was at 6 dB per octave.

The vertical sync signal was also used to open and close a tachistoscopic
shutter placed in front of a 35 mm camera. The vertical sync pulse was
sensed by a specially designed delay/timing circuit which opened and
closed the shutter at specified times after the vertical retrace. The
time between the opening and closing of the shutter was also variable,
but was set at 1/30 s for this research. In this manner, the 35 mm
camera photographed a small portion of a single TV frame.

33

The noise inserted into the video was varied by setting an output potentiometer on the noise generator, the precise output of which was verified by a Ballantine True RMS Voltmeter.

The TV monitor was a Conrac QQA, having a P4 phosphor on a 43 cm (diagonal) CRT. An 11-step gray scale was generated by the TV signal generator to set the monitor's "contrast" and "brightness" controls for maximum gray scale rendition, and to avoid saturation at either end of the luminance range. These procedures have been reported elsewhere (e.g., Keesee, 1976).

35-mm CAMERA AND FILM

The 35 mm camera was a Canon Ftb, equipped with a 50-mm Canon macro lens. Loaded with Kodak Plus X film, the taking lens aperture average f/5.6 at 1/30 s for the photographs in this series. Film development was in Kodak Microdol X at recommended times and temperatures to obtain as close to unity gamma as possible.

It was originally believed that film gamma control would be the key to the utility of this method under the assumption that film *density* within an imaged TV raster line would vary directly with CRT luminance. Initial photographs demonstrated, however, that such was not the case. Rather, increases in luminance along any raster line did not alter appreciably the *luminance* of the raster line, but rather the *width* of the raster line, as shown in figure 13. Thus, the film recording/analysis problem became one of measuring the variation in raster line width rather than line luminance (or film density) as represented on the film frame.

34
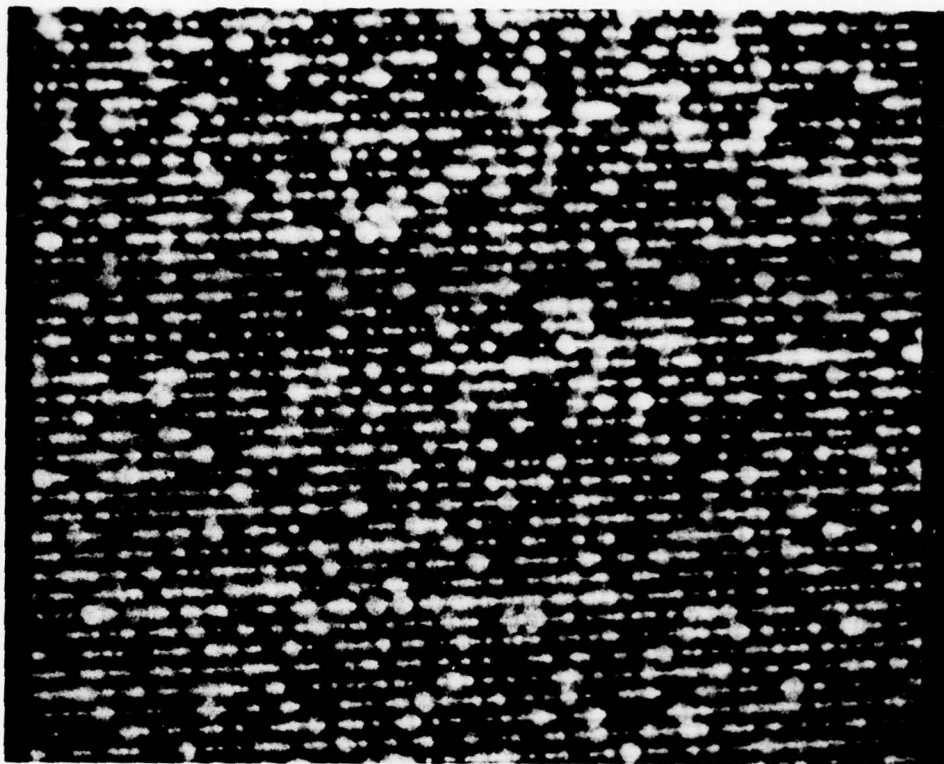
Figure 13.   Enlargement of Noise Modulated Raster Line

MICRODENSITOMETRIC MEASUREMENT

Parameter Selection

In order not to be measurement limited by the filming-microdensitometric process, preliminary experiments were conducted to establish optimum parameters for the filming and the microdensitometric steps.

The centerline-to-centerline spacing of adjacent raster lines on the QQA-15 monitor is 1.061 mm. With the 35 mm camera and its 50 mm macro lens at minimum focusing distance, the centerline-to-centerline raster line image on film was 0.48 mm, for a film image:TV image scale ratio of 1:2.21. The selection of Plus X film permitted a 1/30 s exposure time at an average lens aperture of f/5.6. With this lens aperture/film combination, it is quite doubtful that the film granularity or MTF

35

contributed measurably to the output from the resulting microdensitometric scans of the TV images.

For example, one can show that the film limiting resolution far exceeds the TV bandwidth, as follows. The length of a TV raster line, at the CRT, is approximately 356 mm. At the maximum TV bandwidth of 30 MHz, one can theoretically obtain 1500 TV lines per display width, or 4.3 TVL/mm. At 40 MHz (-6 dB), one obtains 5.6 TVL/mm. For 4.3 TVL/mm, at a film reduction scale of 2.21:1, the required film resolution is 4.65 line pairs/mm. At 5.6 TVL/mm, the required film resolution is 6.19 line pairs/ mm. Since Plus-X film can easily produce over 100 lines/mm, and the MTF for this film is quite flat (at unity) to over 10 lines/mm, there is no effective reduction in the measured TV bandwidth caused by the film scale or MTF. The film granularity, a couple orders of magnitude less ($\sigma_D \simeq$ .03), is totally insignificant at this scale.

Following the above argument, subsequent analyses of the microdensito-metric scans used an upper frequency cutoff of 10 line pairs/mm on the film, which is equivalent to a video bandwidth of nearly 65 MHz.

Previous pilot studies defined the optimal film plane aperture for the microdensitometer to be a rectangular slit with a 4:1 aspect ratio, the longer dimension equal to the maximum width of the raster line (at maximum luminance, as illustrated in figure 13). While this selection was evaluated empirically, the following analysis supports it.

If the scanning is done with a conventional circular aperture, with diameter equal to the width of the raster line, the entire noise modulation at the raster line is accounted for, but the MTF of the

36

microdensitometric scanning process is less than 5% for the highest
frequency the display can provide because of the "large" aperture size
along the image of the raster line. If, on the other hand, the scanning
is done with a small enough circular aperture to maintain, say, 85% MTF
of the video bandwidth, then the aperture cannot account for the entire
modulation (width) of the raster line.

The obvious solution is a rectangular aperture with length equal to
maximum (imaged) raster line width, and aperture width no more than
0.25 of its length. This shape provides an MTF of approximately 90%
at the limiting display resolution. It can be shown that the MTF,
along the raster line, for a circular aperture is given by:

$$\text{MTF}_{circ} = 2\ J_1(\pi\rho f_R)/\pi\rho f_R \ , \tag{10}$$

where

J_1 = the Bessel function of order one,

f_R = the spatial frequency, and

ρ = the radius of the aperture.

For a rectangular aperture of width *a* scanned in the *a* direction, the
MTF is given by:

$$\text{MTF}_{rect} = \text{Sin}(\pi\ a\ f_X)/(\pi\ a\ f_X) = \text{Sinc}(\pi\ a\ f_X)\ , \tag{11}$$

where

f_X = spatial frequency in the *a* direction.

Figure 14 illustrates the MTFs for both rectangular and circular apertures
of 200 μ vertical size. A 50 μ × 200 μ rectangular aperture was used in
this study. With the film image raster line spacing of 480 μ, the 200 μ
slit length essentially "covered" the widest raster line modulation.

37
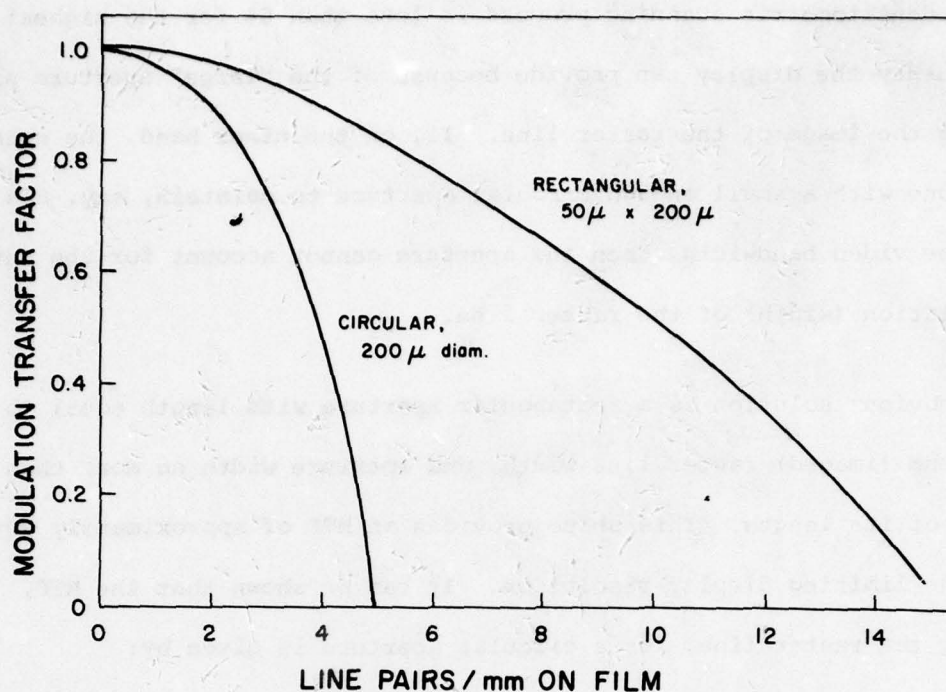
Figure 14. MTFs for Circular and Rectangular Apertures

Longer slit apertures were found to oversample this raster line width,
resulting in less sensitivity; shorter apertures undersampled the line
width, also resulting in less sensitivity. (Of course, this slit size
selection depends on a variety of parameters, such as TV CRT size,
line rate, spot size, 35 mm camera lens, etc. The slit should be
selected specifically for the conditions in any given measurement
situation, a distinct disadvantage to this approach.)

Microdensitometric Procedure

For each TV system configuration, one film frame was taken and processed
to unity gamma. This frame was mounted on the stage of a Gamma
Scientific Model 700-10-80 Microdensitometer, with an illuminated spot
of 50 μ χ 200 μ, described above. The integrating circular eyepiece,
with an effective diameter of 450 μ, overscanned the illuminated spot in

38

the film plane. However, because all room lights were off, it is doubtful that lens flare, film reflections, and the like had any effect on the light entering the 450 μ circular eyepiece.

Three raster lines from each film frame were scanned for a distance of 10 mm, with the analog output from the Model 2400 Digital Photometer recorded directly on magnetic tape through a PDP 11/10 minicomputer and LPS 11 ADC unit. The three scans were chained together in subsequent analyses, yielding an effective sample of 30 mm in the film plane for each experimental condition, or an equivalent CRT raster line distance of over 66 mm.

Experimental Design

Four Noise Passbands (20 Hz - 20 MHz, 20 Hz - 10 MHz, 20 Hz - 5 MHz, and 20 Hz - 2.5 MHz, the same as in the previous study of this report) were combined factorially with four Noise Amplitudes (300, 500, 700, and 1000 mV, RMS) levels to yield a total of 16 experimental conditions. Due to a computer failure, the 20 MHz/1000 mV data were erased, so the resulting analyses are based only on the remaining 15 experimental conditions.

Fourier Transforms of Scan Data

Each noise amplitude/filter combination was scanned three times with the microdensitometer. In the analysis phase, these three scans were added together. The result of the summation process was a 6000-point line which was scaled from 0 to 343 cd/m^2. (An arbitrary photomultiplier gain was used to obtain maximum linearity without saturation. Thus, these luminance values are merely relative units, and cannot be related to CRT luminance.)

The time-weighted average was calculated for each file and removed from each point in the file. This corresponds to removing any DC offset from the scans. Next, the file length was attenuated to equalize end-points to zero. Each file was then Fourier transformed at spatial frequencies of 0.20 to 10.00 cyc/mm in steps of 0.20 cyc/mm. This spatial frequency is referenced to the film surface, as described above.

Power was determined at each frequency by calculating the square root of the sum of the squares of the real and imaginary components at that frequency. The modulation at each frequency was calculated by dividing the power at the frequency by the DC offset.

RESULTS: FILM MICRODENSITOMETRY

POWER DENSITY SPECTRUM ANALYSES

The Fourier transforms provided the power at each spatial frequency for
all 15 experimental conditions. Tables 10 through 24 in the Appendix
list the calculated modulation, power, and average luminance (DC level)
for all scans, with modulation and power calculated in 0.2 cyc/mm steps.
For visual understanding, the power values have been fitted individually
by exponential equations, following a least-squares best-fit criterion.
The accuracy of this curve fitting will be discussed later. Figure 15
illustrates these fitted spectra for the 1000 mV Noise Amplitude condi-
tions, while figures 16 through 18 indicate the spectra for the 700, 500,
and 300 mV levels, respectively.

Noise Amplitude

The power density spectra are affected by Noise Amplitude in an expected
and logical fashion. Power levels for all Noise Passbands generally
increase with increases in Noise Amplitude, as seen by comparing across
figures 15-18. For example, table 8 lists the least-squares, best-fit
equation power at 0.2 cycles/mm for each experimental combination, from
which it can be seen that there is a generally consistent increase in
measured power with increases in Noise Amplitude. The only exception
to this consistent relationship is the 20 Hz - 10 MHz/700 mV combination,
for which no explanation exists.

41
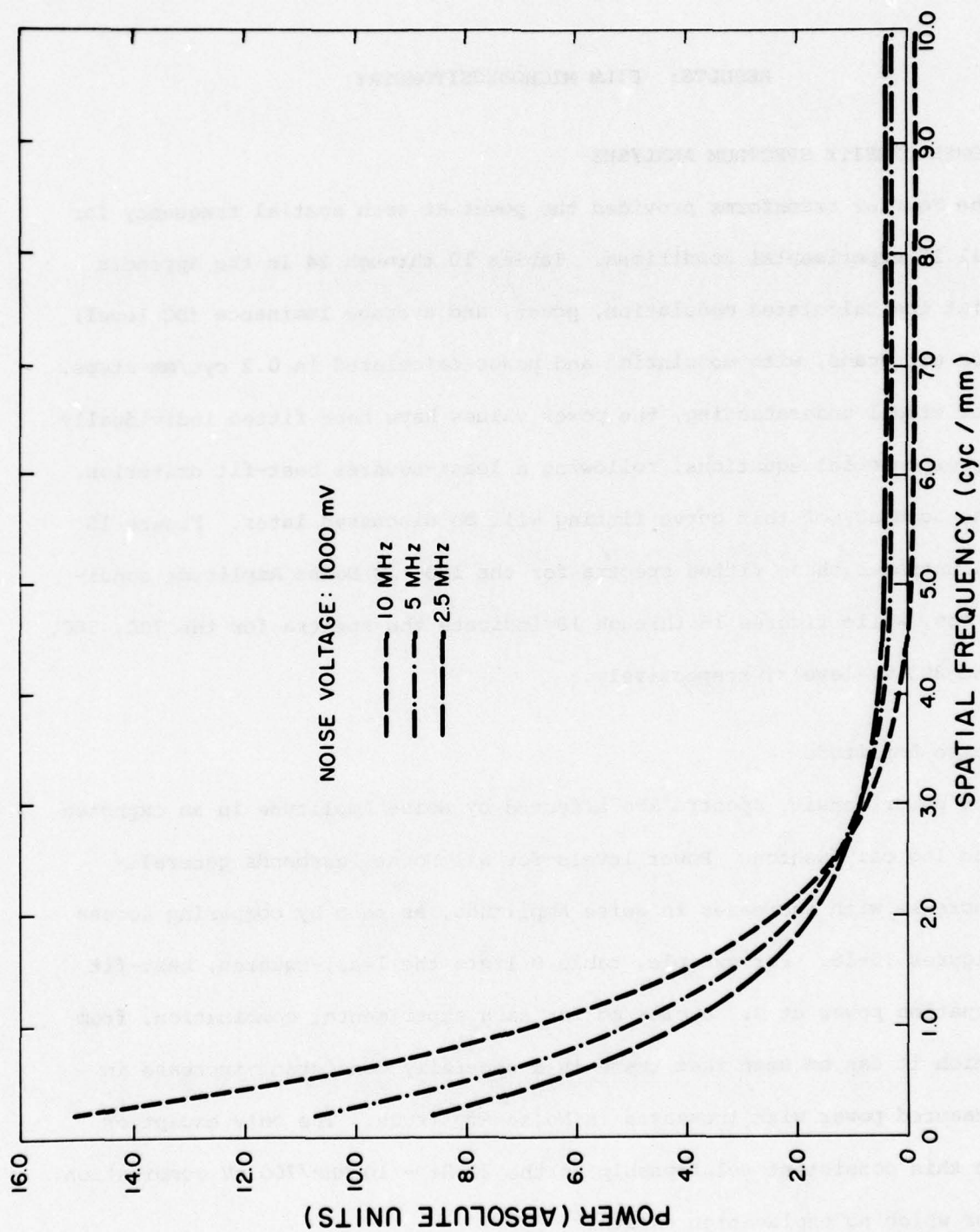
Figure 15. Noise Voltage Spectra, 1000 mV
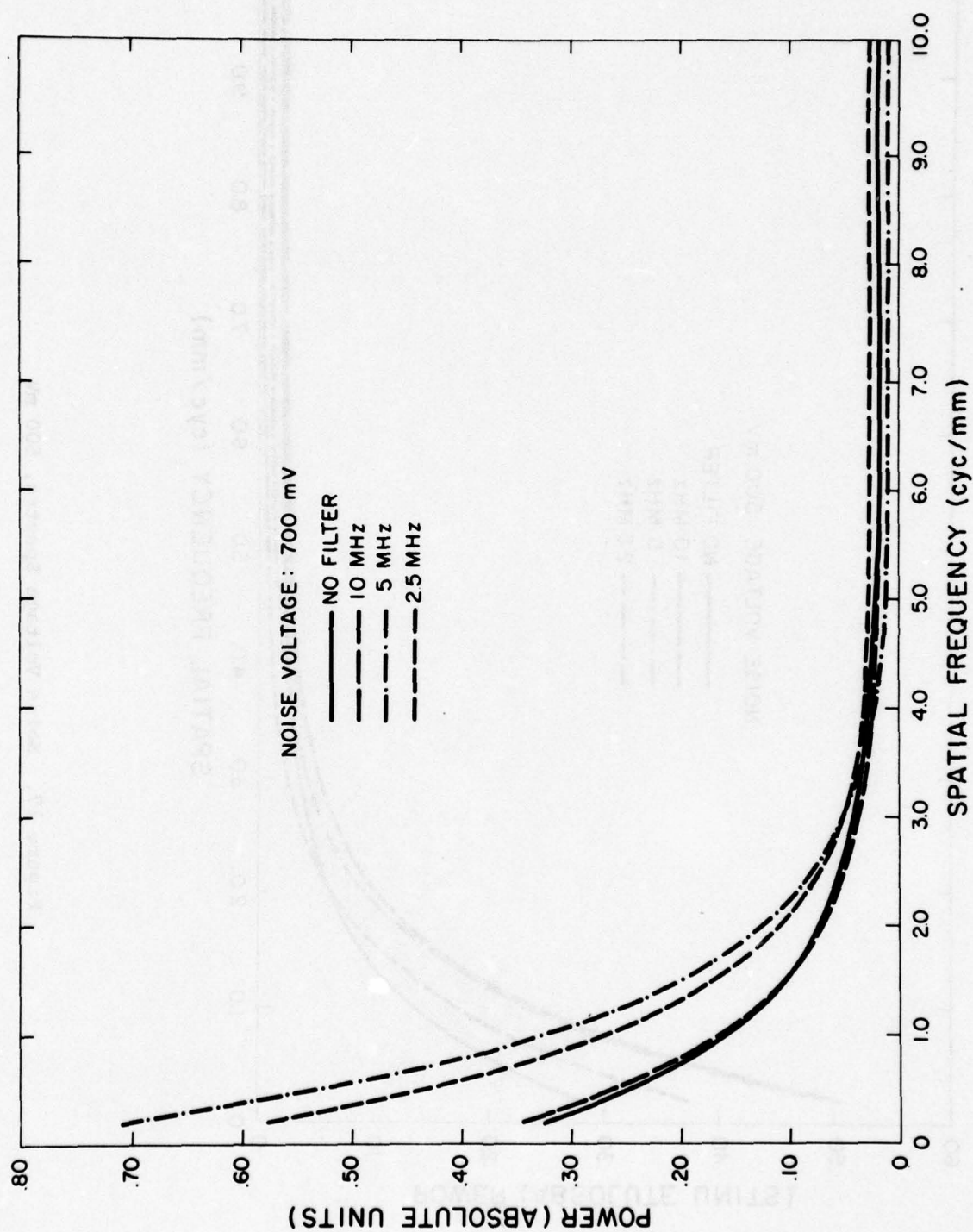
Figure 16. Noise Voltage Spectra, 700 mV

43
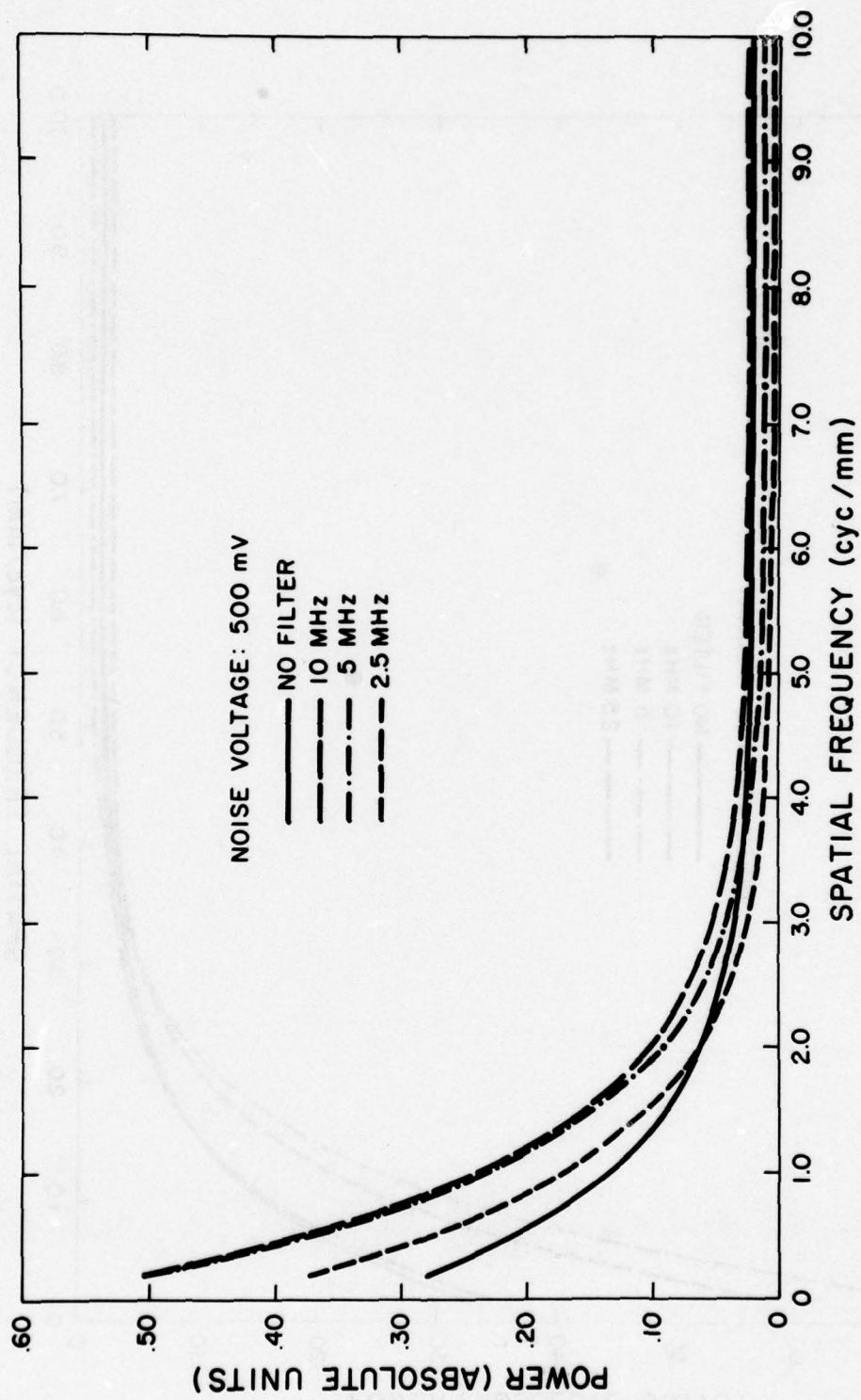
Figure 17. Noise Voltage Spectra, 500 mV

44
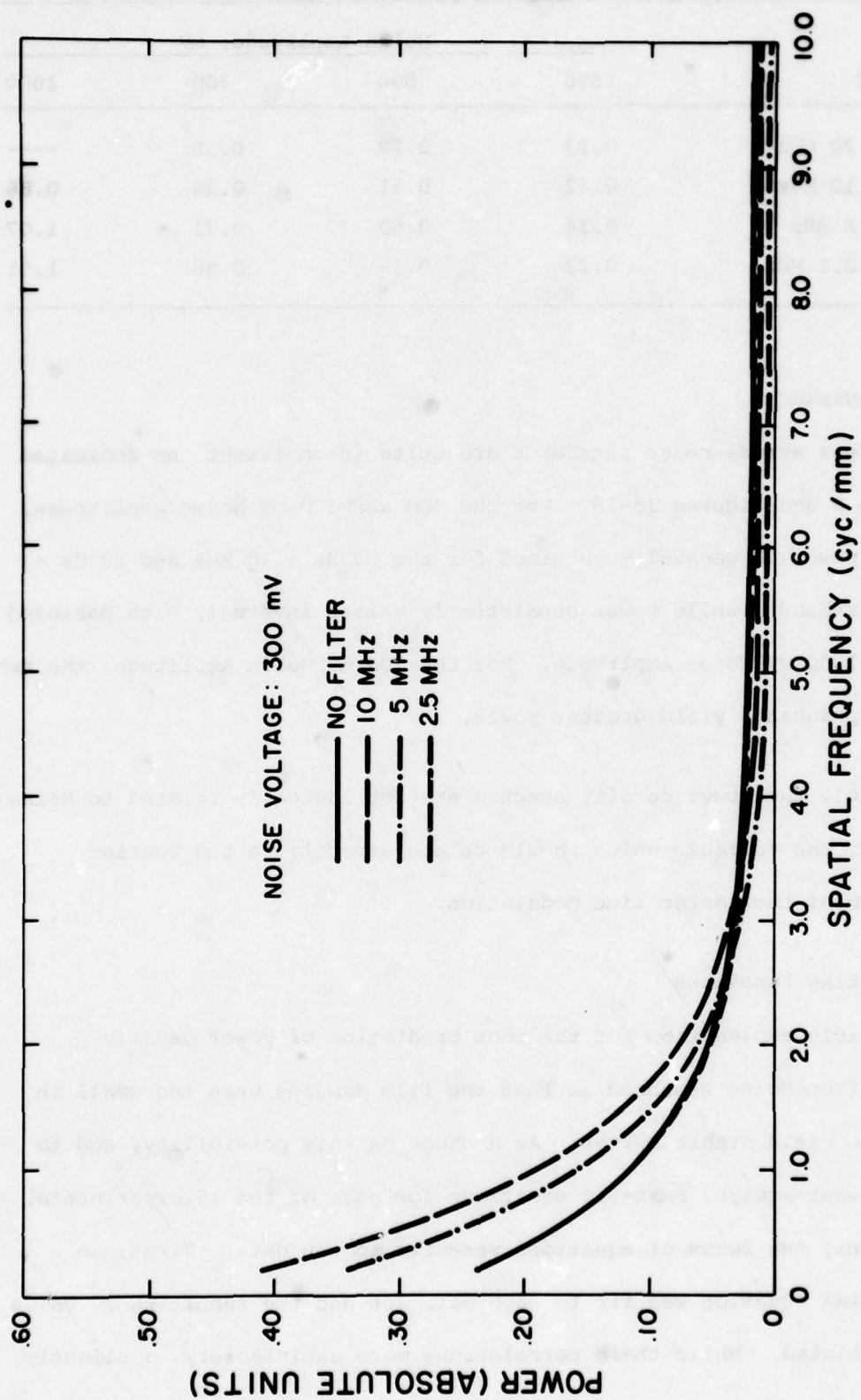
Figure 18. Noise Voltage Spectra, 300 mV

Table 8.   POWER AT 0.2 cyc/mm

Noise Passband	Noise Amplitude, mV			
	300	500	700	1000
20 Hz - 20 MHz	0.23	0.28	0.32	----
20 Hz - 10 MHz	0.42	0.51	0.34	0.86
20 Hz - 5 MHz	0.34	0.50	0.71	1.07
20 Hz - 2.5 MHz	0.23	0.38	0.58	1.51

Noise Passband

Comparisons across noise passbands are quite inconsistent, as indicated
by table 8 and figures 15-18. For the 300 and 500 mV Noise Amplitudes,
maximum power is generally obtained for the 20 Hz - 10 MHz and 20 Hz -
5 MHz passbands, while power consistently varies inversely with passband
for the 1000 mV Noise Amplitude. For the 700 mV Noise Amplitude, the two
smaller passbands yield greater power.

In general, the power density spectra are not logically related to Noise
Passband, the variable which should relate directly to the Fourier
transform of the raster line modulation.

Best-Fitting Functions

One possible explanation for the poor prediction of power density
spectra from Noise Passband is that the film samples were too small in
number to yield stable curves. As a check on this possibility, and to
obtain least-squares best-fit equations for each of the 15 experimental
conditions, two forms of equations were fit to the data. First, an
exponential equation was fit to each data set and the resulting r^2 value
was calculated. While these correlations were satisfactory, a slightly

46

better fit was obtained by a combined linear plus exponential equation. R^2 values for both, and coefficients for the linear plus exponential form, are given in table 9.

Table 9. PREDICTED VARIANCE (R^2) FOR POWER DENSITY SPECTRA EQUATIONS

Noise Amp.	Noise Passband, Hz	Predicted Variance (%)		Best-Fit Coefficients[a]		
		Exponential	Linear + Exponential	-E	A	I
1000 mV	20 - 10 M	79	79	1.0087	---	0.0359
	20 - 5 M	83	83	1.2778	---	0.0283
	20 - 2.5 M	79	81	2.1192	0.0232	-0.1582
700 mV	20 - 20 M	66	72	0.2574	-0.0095	0.0845
	20 - 10 M	87	88	0.3995	---	0.0168
	20 - 5 M	91	91	0.8557	---	0.0088
	20 - 2.5 M	81	81	0.6863	---	0.0164
500 mV	20 - 20 M	75	76	0.3176	---	0.0190
	20 - 10 M	69	69	0.5942	---	0.0220
	20 - 5 M	85	85	0.6008	---	0.0110
	20 - 2.5 M	79	80	0.4525	---	0.0033
300 mV	20 - 20 M	84	84	0.2670	---	0.0166
	20 - 10 M	75	76	0.4890	---	0.0111
	20 - 5 M	88	88	0.4136	---	0.0049
	20 - 2.5 M	83	83	0.2709	---	0.0136

[a] Best-fit equation is of the form: Noise Power = $(SF)^{-E} + A(SF) + I$, where SF is spatial frequency in cycles/mm on film.

As indicated in table 9, the least-squares best-fit equations predict a minimum of 69% of the variation in power, and average approximately 81% in prediction. Thus, prediction equations can be fit accurately to the data, and any inconsistencies in the effects of the two independent variables are not due to random measurement error.

47

RMS Luminance

It was hoped that the microdensitometric scans could be sampled
periodically (e.g., each of the sampled data points that were used
in the Fourier transform) with the standard deviation of these samples
calculated to yield an estimate of RMS luminance on the CRT. However,
closer examination of the problem showed this procedure to be inappro-
priate because the integrating slit of the microdensitometer sampled
outside the raster line for all but maximum raster modulation levels.
Thus, the photomultiplier tube output could not be calibrated in terms
of absolute luminance at the CRT; rather, only power and modulation,
both relative units, were obtainable. In view of the disappointing
power density spectra results, it is doubtful that RMS luminance values,
if they could be calculated from the film images, would be very useful
or reliable.

DISCUSSION AND SUMMARY

Of the two techniques investigated for the direct measurement of
photometric noise on the raster-scan display, the spot microphotometry
technique is clearly superior, for several reasons.

First, it is easier to implement in that (1) no special slit aperture
needs to be developed for a microdensitometer for each CRT/photographic
lens combination; (2) the film processing, microdensitometric scan
procedure is avoided, which is a long, laborious procedure; and (3) the
RMS luminance calculation is simpler and requires less sophisticated
data processing than the Fourier transform technique.

Secondly, the spot microphotometry technique appears to yield valid,
accurate results for a variety of display conditions, whereas the film
microdensitometry technique produces results inconsistent with known
display input conditions.

For these reasons, the spot microphotometry approach is recommended for
siutations in which input noise cannot be measured or when it is desir-
able to measure display noise (phosphor, voltage fluctuation, etc.)
which cannot be seen on the electrical input signal. In point of fact,
such displayed noise *does* exist, even when electrical input noise is
zero, as illustrated in figures 7-9.

Based upon the results of the first experiment described in this report,
the optimal measurement conditions for spot microphotometric noise

measurement can be described as follows.

1. The sampling aperture should be on the order of 112 μ for a raster line spacing of 0.29 mm. In this study, this aperture provided the greatest, most consistent sensitivity (figure 11) and the highest linearity (r^2 = 0.974) with known input noise (figure 9).

2. RMS luminance measurements are more sensitive for higher display average luminance levels. This is not at all surprising, since RMS values and means of any random variables are highly correlated; nonetheless, it does point out the dependence of the RMS noise upon display mean luminance.

3. The wider the video bandwidth, the more sensitive is the RMS luminance measurement, as indicated in figures 8 and 10. The authors know of no logical proof for this result, although it appears consistent in the data.

In summary, the spot microphotometry approach appears valid, reliable, and meaningful. It is recommended whenever the display designer or researcher must evaluate photometrically the noise on a raster scan display.

APPENDIX:

MEASURED MODULATION FOR MICRODENSITOMETRY EXPERIMENT

Tables 10 through 24 list the modulation and power, as a function of spatial frequency (in the film plane), for each condition of the microdensitometry experiment.

Table 10. MODULATION AND POWER AS A FUNCTION OF SPATIAL FREQUENCY: 1000 mV, 20 Hz – 10 MHz

Spatial Frequency (cyc/mm)	Modulation	Power	Spatial Frequency (cyc/mm)	Modulation	Power
0.20	0.0193	1.1132	5.20	0.0007	0.0386
0.40	0.0073	0.4199	5.40	0.0003	0.0154
0.60	0.0051	0.2937	5.60	0.0003	0.0178
0.80	0.0116	0.6715	5.80	0.0001	0.0046
1.00	0.0051	0.2964	6.00	0.0008	0.0467
1.20	0.0079	0.4582	6.20	0.0008	0.0479
1.40	0.0061	0.3528	6.40	0.0003	0.0153
1.60	0.0036	0.2062	6.60	0.0006	0.0331
1.80	0.0092	0.5316	6.80	0.0006	0.0332
2.00	0.0040	0.2287	7.00	0.0002	0.0114
2.20	0.0024	0.1404	7.20	0.0006	0.0350
2.40	0.0034	0.1946	7.40	0.0006	0.0328
2.60	0.0013	0.0777	7.60	0.0003	0.0156
2.80	0.0019	0.1117	7.80	0.0002	0.0115
3.00	0.0020	0.1181	8.00	0.0005	0.0275
3.20	0.0004	0.0245	8.20	0.0003	0.0189
3.40	0.0014	0.0833	8.40	0.0007	0.0385
3.60	0.0008	0.0448	8.60	0.0003	0.0162
3.80	0.0009	0.0544	8.80	0.0005	0.0286
4.00	0.0010	0.0605	9.00	0.0002	0.0104
4.20	0.0008	0.0455	9.20	0.0003	0.0197
4.40	0.0012	0.0685	9.40	0.0001	0.0067
4.60	0.0009	0.0515	9.60	0.0002	0.0112
4.80	0.0019	0.1087	9.80	0.0002	0.0108
5.00	0.0006	0.0340	10.00	0.0002	0.0139

Table 11. MODULATION AND POWER AS A FUNCTION OF SPATIAL FREQUENCY: 1000 mV, 20 Hz - 5 MHz

Spatial Frequency (cyc/mm)	Modulation	Power	Spatial Frequency (cyc/mm)	Modulation	Power
0.20	0.0148	0.8476	5.20	0.0001	0.0067
0.40	0.0100	1.1436	5.40	0.0004	0.0228
0.60	0.0184	1.0523	5.60	0.0005	0.0291
0.80	0.0057	0.3267	5.80	0.0002	0.0139
1.00	0.0067	0.3822	6.00	0.0012	0.0673
1.20	0.0036	0.2081	6.20	0.0003	0.0163
1.40	0.0114	0.6493	6.40	0.0003	0.0169
1.60	0.0032	0.1811	6.60	0.0010	0.0575
1.80	0.0036	0.2054	6.80	0.0006	0.0317
2.00	0.0031	0.1781	7.00	0.0005	0.0308
2.20	0.0060	0.3441	7.20	0.0004	0.0229
2.40	0.0029	0.1647	7.40	0.0005	0.0258
2.60	0.0011	0.0612	7.60	0.0006	0.0358
2.80	0.0011	0.0624	7.80	0.0005	0.0300
3.00	0.0027	0.1534	8.00	0.0006	0.0357
3.20	0.0005	0.0305	8.20	0.0004	0.0217
3.40	0.0030	0.1735	8.40	0.0002	0.0086
3.60	0.0011	0.0609	8.60	0.0004	0.0252
3.80	0.0004	0.0249	8.80	0.0004	0.0245
4.00	0.0005	0.0286	9.00	0.0005	0.0262
4.20	0.0017	0.0972	9.20	0.0003	0.0190
4.40	0.0006	0.0352	9.40	0.0002	0.0123
4.60	0.0007	0.0419	9.60	0.0003	0.0174
4.80	0.0008	0.0467	9.80	0.0001	0.0042
5.00	0.0011	0.0653	10.00	0.0003	0.0167

Table 12. MODULATION AND POWER AS A FUNCTION OF SPATIAL FREQUENCY: 1000 mV, 20 Hz - 2.5 MHz

Spatial Frequency (cyc/mm)	Modulation	Power	Spatial Frequency (cyc/mm)	Modulation	Power
0.20	0.0239	1.1586	5.20	0.0003	0.0161
0.40	0.0439	2.1254	5.40	0.0004	0.0216
0.60	0.0237	1.1481	5.60	0.0005	0.0263
0.80	0.0152	0.7336	5.80	0.0005	0.0261
1.00	0.0120	0.5791	6.00	0.0007	0.0323
1.20	0.0004	0.0182	6.20	0.0003	0.0134
1.40	0.0050	0.2416	6.40	0.0002	0.0109
1.60	0.0042	0.2010	6.60	0.0008	0.0409
1.80	0.0014	0.0659	6.80	0.0003	0.0146
2.00	0.0013	0.0627	7.00	0.0007	0.0320
2.20	0.0018	0.0848	7.20	0.0005	0.0248
2.40	0.0037	0.1792	7.40	0.0009	0.0417
2.60	0.0006	0.0312	7.60	0.0006	0.0279
2.80	0.0004	0.0198	7.80	0.0004	0.0194
3.00	0.0012	0.0581	8.00	0.0004	0.0210
3.20	0.0015	0.0724	8.20	0.0001	0.0038
3.40	0.0009	0.0434	8.40	0.0003	0.0165
3.60	0.0006	0.0277	8.60	0.0003	0.0137
3.80	0.0004	0.0215	8.80	0.0005	0.0266
4.00	0.0012	0.0564	9.00	0.0006	0.0284
4.20	0.0014	0.0665	9.20	0.0004	0.0205
4.40	0.0007	0.0358	9.40	0.0000	0.0010
4.60	0.0002	0.0114	9.60	0.0002	0.0094
4.80	0.0005	0.0237	9.80	0.0004	0.0203
5.00	0.0001	0.0068	10.00	0.0003	0.0144

Table 13. MODULATION AND POWER AS A FUNCTION OF SPATIAL FREQUENCY: 700 mV, 20 Hz - 20 MHz

Spatial Frequency (cyc/mm)	Modulation	Power	Spatial Frequency (cyc/mm)	Modulation	Power
0.20	0.0025	0.1812	5.20	0.0002	0.0162
0.40	0.0043	0.3097	5.40	0.0003	0.0240
0.60	0.0009	0.0632	5.60	0.0003	0.0244
0.80	0.0032	0.2262	5.80	0.0005	0.0387
1.00	0.0050	0.3545	6.00	0.0003	0.0199
1.20	0.0001	0.0077	6.20	0.0001	0.0093
1.40	0.0037	0.2620	6.40	0.0002	0.0123
1.60	0.0014	0.1008	6.60	0.0004	0.0261
1.80	0.0010	0.0701	6.80	0.0002	0.0123
2.00	0.0011	0.0772	7.00	0.0003	0.0165
2.20	0.0017	0.1194	7.20	0.0003	0.0212
2.40	0.0025	0.1753	7.40	0.0001	0.0092
2.60	0.0008	0.0538	7.60	0.0002	0.0154
2.80	0.0006	0.0399	7.80	0.0000	0.0027
3.00	0.0020	0.1440	8.00	0.0002	0.0136
3.20	0.0011	0.0808	8.20	0.0003	0.0212
3.40	0.0006	0.0429	8.40	0.0003	0.0156
3.60	0.0005	0.0365	8.60	0.0002	0.0176
3.80	0.0007	0.0479	8.80	0.0001	0.0044
4.00	0.0002	0.0144	9.00	0.0000	0.0019
4.20	0.0005	0.0332	9.20	0.0002	0.0145
4.40	0.0003	0.0184	9.40	0.0002	0.0134
4.60	0.0010	0.0739	9.60	0.0001	0.0053
4.80	0.0002	0.0110	9.80	0.0001	0.0084
5.00	0.0004	0.0257	10.00	0.0002	0.0143

Table 14. MODULATION AND POWER AS A FUNCTION OF SPATIAL FREQUENCY: 700 mV, 20 Hz – 10 MHz

Spatial Frequency (cyc/mm)	Modulation	Power	Spatial Frequency (cyc/mm)	Modulation	Power
0.20	0.0056	0.4043	5.20	0.0009	0.0615
0.40	0.0040	0.2838	5.40	0.0001	0.0052
0.60	0.0027	0.1921	5.60	0.0000	0.0006
0.80	0.0014	0.0989	5.80	0.0002	0.0156
1.00	0.0024	0.1723	6.00	0.0002	0.0131
1.20	0.0019	0.1373	6.20	0.0007	0.0508
1.40	0.0018	0.1312	6.40	0.0002	0.0110
1.60	0.0011	0.0810	6.60	0.0001	0.0072
1.80	0.0009	0.0612	6.80	0.0002	0.0148
2.00	0.0020	0.1459	7.00	0.0000	0.0024
2.20	0.0018	0.1288	7.20	0.0003	0.0243
2.40	0.0008	0.0584	7.40	0.0005	0.0372
2.60	0.0005	0.0372	7.60	0.0002	0.0168
2.80	0.0013	0.0964	7.80	0.0002	0.0120
3.00	0.0002	0.0112	8.00	0.0001	0.0047
3.20	0.0001	0.0097	8.20	0.0001	0.0075
3.40	0.0002	0.0143	8.40	0.0002	0.0129
3.60	0.0003	0.0250	8.60	0.0000	0.0022
3.80	0.0003	0.0200	8.80	0.0001	0.0051
4.00	0.0007	0.0501	9.00	0.0001	0.0095
4.20	0.0004	0.0301	9.20	0.0003	0.0222
4.40	0.0001	0.0104	9.40	0.0001	0.0091
4.60	0.0004	0.0292	9.60	0.0002	0.0129
4.80	0.0004	0.0255	9.80	0.0002	0.0116
5.00	0.0002	0.0141	10.00	0.0001	0.0037

Table 15. MODULATION AND POWER AS A FUNCTION OF SPATIAL FREQUENCY: 700 mV, 20 Hz - 5 MHz

Spatial Frequency (cyc/mm)	Modulation	Power	Spatial Frequency (cyc/mm)	Modulation	Power
0.20	0.0126	0.8259	5.20	0.0004	0.0242
0.40	0.0094	0.6158	5.40	0.0007	0.0457
0.60	0.0049	0.3233	5.60	0.0004	0.0232
0.80	0.0039	0.2559	5.80	0.0005	0.0313
1.00	0.0068	0.4465	6.00	0.0001	0.0076
1.20	0.0051	0.3374	6.20	0.0002	0.0150
1.40	0.0033	0.2179	6.40	0.0001	0.0034
1.60	0.0009	0.0620	6.60	0.0001	0.0062
1.80	0.0012	0.0780	6.80	0.0001	0.0065
2.00	0.0020	0.1341	7.00	0.0002	0.0139
2.20	0.0022	0.1472	7.20	0.0001	0.0043
2.40	0.0003	0.0197	7.40	0.0002	0.0129
2.60	0.0006	0.0389	7.60	0.0001	0.0097
2.80	0.0002	0.0142	7.80	0.0001	0.0092
3.00	0.0013	0.0830	8.00	0.0000	0.0030
3.20	0.0003	0.0188	8.20	0.0001	0.0090
3.40	0.0016	0.1067	8.40	0.0002	0.0135
3.60	0.0006	0.0404	8.60	0.0000	0.0027
3.80	0.0002	0.1414	8.80	0.0003	0.0174
4.00	0.0008	0.0522	9.00	0.0002	0.0123
4.20	0.0005	0.0325	9.20	0.0002	0.0121
4.40	0.0007	0.0465	9.40	0.0001	0.0084
4.60	0.0005	0.0357	9.60	0.0000	0.0032
4.80	0.0001	0.0092	9.80	0.0001	0.0053
5.00	0.0006	0.0395	10.00	0.0002	0.0100

57

Table 16. MODULATION AND POWER AS A FUNCTION OF SPATIAL FREQUENCY: 700 mV   20 Hz – 2.5 MHz

Spatial Frequency (cyc/mm)	Modulation	Power	Spatial Frequency (cyc/mm)	Modulation	Power
0.20	0.0094	0.6532	5.20	0.0005	0.0334
0.40	0.0038	0.2665	5.40	0.0002	0.0143
0.60	0.0034	0.2369	5.60	0.0003	0.0188
0.80	0.0064	0.4453	5.80	0.0002	0.0112
1.00	0.0065	0.4474	6.00	0.0002	0.0107
1.20	0.0062	0.4312	6.20	0.0001	0.0057
1.40	0.0031	0.2122	6.40	0.0006	0.0434
1.60	0.0024	0.1656	6.60	0.0000	0.0034
1.80	0.0005	0.0332	6.80	0.0003	0.0210
2.00	0.0013	0.0927	7.00	0.0004	0.0276
2.20	0.0005	0.0337	7.20	0.0001	0.0098
2.40	0.0007	0.0489	7.40	0.0001	0.0086
2.60	0.0010	0.0707	7.60	0.0002	0.0146
2.80	0.0010	0.0718	7.80	0.0002	0.0132
3.00	0.0006	0.0441	8.00	0.0002	0.0126
3.20	0.0010	0.0709	8.20	0.0001	0.0070
3.40	0.0002	0.0154	8.40	0.0002	0.0151
3.60	0.0008	0.0527	8.60	0.0003	0.0200
3.80	0.0005	0.0377	8.80	0.0001	0.0060
4.00	0.0004	0.0276	9.00	0.0002	0.0168
4.20	0.0006	0.0400	9.20	0.0002	0.0149
4.40	0.0001	0.0096	9.40	0.0001	0.0098
4.60	0.0003	0.0220	9.60	0.0002	0.0143
4.80	0.0002	0.0121	9.80	0.0002	0.0141
5.00	0.0001	0.0084	10.00	0.0001	0.0054

58

Table 17. MODULATION AND POWER AS A FUNCTION OF SPATIAL FREQUENCY: 500 mV, 20 Hz - 20 MHz

Spatial Frequency (cyc/mm)	Modulation	Power	Spatial Frequency (cyc/mm)	Modulation	Power
0.20	0.0056	0.3556	5.20	0.0003	0.0169
0.40	0.0042	0.2636	5.40	0.0005	0.0291
0.60	0.0011	0.0696	5.60	0.0005	0.0307
0.80	0.0021	0.1360	5.80	0.0001	0.0094
1.00	0.0031	0.1948	6.00	0.0005	0.0306
1.20	0.0011	0.0729	6.20	0.0005	0.0288
1.40	0.0003	0.0206	6.40	0.0001	0.0056
1.60	0.0008	0.0508	6.60	0.0005	0.0292
1.80	0.0005	0.0290	6.80	0.0002	0.0146
2.00	0.0020	0.1289	7.00	0.0003	0.0193
2.20	0.0015	0.0978	7.20	0.0003	0.0162
2.40	0.0006	0.0399	7.40	0.0002	0.0130
2.60	0.0016	0.1915	7.60	0.0004	0.0252
2.80	0.0001	0.0090	7.80	0.0003	0.0199
3.00	0.0009	0.0569	8.00	0.0001	0.0077
3.20	0.0005	0.0290	8.20	0.0004	0.0277
3.40	0.0008	0.0505	8.40	0.0001	0.0084
3.60	0.0009	0.0582	8.60	0.0001	0.0042
3.80	0.0003	0.0169	8.80	0.0002	0.0105
4.00	0.0007	0.0430	9.00	0.0001	0.0057
4.20	0.0005	0.0323	9.20	0.0001	0.0055
4.40	0.0007	0.0427	9.40	0.0001	0.0071
4.60	0.0004	0.0281	9.60	0.0002	0.0135
4.80	0.0008	0.0485	9.80	0.0001	0.0057
5.00	0.0003	0.0199	10.00	0.0001	0.0058

59

Table 18. MODULATION AND POWER AS A FUNCTION OF SPATIAL FREQUENCY: 500 mV, 20 Hz - 10 MHz

Spatial Frequency (cyc/mm)	Modulation	Power	Spatial Frequency (cyc/mm)	Modulation	Power
0.20	0.0045	0.2794	5.20	0.0007	0.0422
0.40	0.0101	0.6322	5.40	0.0005	0.0343
0.60	0.0075	0.4714	5.60	0.0005	0.0286
0.80	0.0015	0.0911	5.80	0.0005	0.0316
1.00	0.0083	0.5178	6.00	0.0003	0.0167
1.20	0.0016	0.0995	6.20	0.0003	0.0182
1.40	0.0015	0.0910	6.40	0.0005	0.0325
1.60	0.0019	0.1201	6.60	0.0003	0.0206
1.80	0.0023	0.1426	6.80	0.0003	0.0182
2.00	0.0025	0.1559	7.00	0.0002	0.0148
2.20	0.0015	0.0953	7.20	0.0002	0.0117
2.40	0.0025	0.1553	7.40	0.0002	0.0110
2.60	0.0006	0.0398	7.60	0.0005	0.0284
2.80	0.0012	0.0747	7.80	0.0002	0.0132
3.00	0.0011	0.0706	8.00	0.0002	0.0105
3.20	0.0004	0.0257	8.20	0.0001	0.0043
3.40	0.0009	0.0579	8.40	0.0002	0.0120
3.60	0.0008	0.0501	8.60	0.0001	0.0034
3.80	0.0003	0.0163	8.80	0.0002	0.0136
4.00	0.0004	0.0238	9.00	0.0001	0.0064
4.20	0.0004	0.0256	9.20	0.0001	0.0077
4.40	0.0006	0.0353	9.40	0.0001	0.0081
4.60	0.0005	0.0293	9.60	0.0001	0.0093
4.80	0.0003	0.0179	9.80	0.0001	0.0070
5.00	0.0008	0.0528	10.00	0.0001	0.0057

Table 19. MODULATION AND POWER AS A FUNCTION OF SPATIAL FREQUENCY: 500 mV, 20 Hz - 5 MHz

Spatial Frequency (cyc/mm)	Modulation	Power	Spatial Frequency (cyc/mm)	Modulation	Power
0.20	0.0111	0.0684	5.20	0.0001	0.0084
0.40	0.0039	0.2414	5.40	0.0003	0.0178
0.60	0.0041	0.2532	5.60	0.0003	0.0189
0.80	0.0058	0.3584	5.80	0.0001	0.0067
1.00	0.0049	0.2993	6.00	0.0005	0.0311
1.20	0.0017	0.1038	6.20	0.0006	0.0366
1.40	0.0026	0.1603	6.40	0.0004	0.0217
1.60	0.0006	0.0391	6.60	0.0004	0.0216
1.80	0.0014	0.0863	6.80	0.0003	0.0196
2.00	0.0013	0.0818	7.00	0.0002	0.0116
2.20	0.0016	0.0996	7.20	0.0003	0.0192
2.40	0.0005	0.0311	7.40	0.0003	0.0175
2.60	0.0019	0.1155	7.60	0.0003	0.0168
2.80	0.0011	0.0657	7.80	0.0004	0.0227
3.00	0.0006	0.0355	8.00	0.0000	0.0008
3.20	0.0011	0.0655	8.20	0.0004	0.0249
3.40	0.0007	0.0405	8.40	0.0000	0.0010
3.60	0.0004	0.0252	8.60	0.0001	0.0090
3.80	0.0005	0.0324	8.80	0.0000	0.0015
4.00	0.0006	0.0356	9.00	0.0001	0.0069
4.20	0.0003	0.0185	9.20	0.0001	0.0053
4.40	0.0001	0.0062	9.40	0.0002	0.0093
4.60	0.0002	0.0113	9.60	0.0001	0.0082
4.80	0.0002	0.0119	9.80	0.0001	0.0079
5.00	0.0003	0.0163	10.00	0.0000	0.0014

Table 20. MODULATION AND POWER AS A FUNCTION OF SPATIAL FREQUENCY: 500 mV, 20 Hz - 2.5 MHz

Spatial Frequency (cyc/mm)	Modulation	Power	Spatial Frequency (cyc/mm)	Modulation	Power
0.20	0.0062	0.4271	5.20	0.0005	0.0365
0.40	0.0030	0.2034	5.40	0.0000	0.0028
0.60	0.0068	0.4692	5.60	0.0002	0.0123
0.80	0.0013	0.0863	5.80	0.0002	0.0138
1.00	0.0022	0.1500	6.00	0.0001	0.0079
1.20	0.0020	0.1400	6.20	0.0001	0.0087
1.40	0.0009	0.0645	6.40	0.0001	0.0043
1.60	0.0011	0.0691	6.60	0.0001	0.0094
1.80	0.0004	0.0258	6.80	0.0003	0.0225
2.00	0.0003	0.0182	7.00	0.0000	0.0024
2.20	0.0007	0.0475	7.20	0.0002	0.0137
2.40	0.0008	0.0572	7.40	0.0001	0.0096
2.60	0.0001	0.0044	7.60	0.0001	0.0103
2.80	0.0002	0.0120	7.80	0.0001	0.0057
3.00	0.0001	0.0061	8.00	0.0001	0.0050
3.20	0.0006	0.0448	8.20	0.0001	0.0067
3.40	0.0003	0.0177	8.40	0.0001	0.0067
3.60	0.0003	0.0191	8.60	0.0002	0.0122
3.80	0.0002	0.0107	8.80	0.0001	0.0035
4.00	0.0003	0.0191	9.00	0.0001	0.0064
4.20	0.0002	0.0162	9.20	0.0001	0.0056
4.40	0.0004	0.0261	9.40	0.0001	0.0050
4.60	0.0003	0.0178	9.60	0.0000	0.0010
4.80	0.0001	0.0092	9.80	0.0001	0.0044
5.00	0.0001	0.0082	10.00	0.0002	0.0123

Table 21. MODULATION AND POWER AS A FUNCTION OF SPATIAL FREQUENCY: 300 mV, 20 Hz - 20 MHz

Spatial Frequency (cyc/mm)	Modulation	Power	Spatial Frequency (cyc/mm)	Modulation	Power
0.20	0.0043	0.2457	5.20	0.0006	0.0320
0.40	0.0040	0.2266	5.40	0.0006	0.0327
0.60	0.0029	0.1658	5.60	0.0001	0.0083
0.80	0.0019	0.1065	5.80	0.0003	0.0147
1.00	0.0017	0.0992	6.00	0.0003	0.0188
1.20	0.0005	0.0284	6.20	0.0004	0.0233
1.40	0.0011	0.0613	6.40	0.0005	0.0297
1.60	0.0012	0.0670	6.60	0.0001	0.0039
1.80	0.0021	0.1214	6.80	0.0002	0.0102
2.00	0.0011	0.0609	7.00	0.0002	0.0128
2.20	0.0015	0.0861	7.20	0.0001	0.0060
2.40	0.0013	0.0760	7.40	0.0003	0.0156
2.60	0.0001	0.0057	7.60	0.0003	0.0181
2.80	0.0015	0.0827	7.80	0.0002	0.0115
3.00	0.0006	0.0344	8.00	0.0003	0.0193
3.20	0.0012	0.0706	8.20	0.0001	0.0033
3.40	0.0001	0.0066	8.40	0.0001	0.0054
3.60	0.0006	0.0354	8.60	0.0001	0.0084
3.80	0.0002	0.0120	8.80	0.0001	0.0057
4.00	0.0003	0.0164	9.00	0.0004	0.0252
4.20	0.0001	0.0071	9.20	0.0004	0.0216
4.40	0.0007	0.0424	9.40	0.0002	0.0101
4.60	0.0003	0.0194	9.60	0.0001	0.0072
4.80	0.0002	0.0117	9.80	0.0001	0.0043
5.00	0.0001	0.0035	10.00	0.0001	0.0065

Table 22. MODULATION AND POWER AS A FUNCTION OF SPATIAL FREQUENCY: 300 mV, 20 Hz – 10 MHz

Spatial Frequency (cyc/mm)	Modulation	Power	Spatial Frequency (cyc/mm)	Modulation	Power
0.20	0.0115	0.6407	5.20	0.0006	0.0320
0.40	0.0066	0.2691	5.40	0.0003	0.0180
0.60	0.0029	0.1612	5.60	0.0004	0.0229
0.80	0.0031	0.1753	5.80	0.0006	0.0359
1.00	0.0006	0.0322	6.00	0.0003	0.0194
1.20	0.0014	0.0791	6.20	0.0002	0.0087
1.40	0.0012	0.0659	6.40	0.0007	0.0399
1.60	0.0008	0.0455	6.60	0.0001	0.0039
1.80	0.0005	0.0256	6.80	0.0002	0.0118
2.00	0.0011	0.0623	7.00	0.0002	0.0126
2.20	0.0008	0.0425	7.20	0.0003	0.0143
2.40	0.0006	0.0315	7.40	0.0003	0.0140
2.60	0.0006	0.0349	7.60	0.0003	0.0156
2.80	0.0012	0.0654	7.80	0.0002	0.0088
3.00	0.0007	0.0372	8.00	0.0003	0.0142
3.20	0.0008	0.0442	8.20	0.0004	0.0198
3.40	0.0014	0.0806	8.40	0.0004	0.0228
3.60	0.0014	0.0794	8.60	0.0004	0.0223
3.80	0.0014	0.0788	8.80	0.0002	0.0126
4.00	0.0005	0.0295	9.00	0.0001	0.0057
4.20	0.0009	0.0490	9.20	0.0002	0.0139
4.40	0.0003	0.0155	9.40	0.0001	0.0048
4.60	0.0003	0.0169	9.60	0.0002	0.0114
4.80	0.0006	0.0316	9.80	0.0002	0.0122
5.00	0.0007	0.0412	10.00	0.0002	0.0103

Table 23. MODULATION AND POWER AS A FUNCTION OF SPATIAL FREQUENCY: 300 mV, 20 Hz – 5 MHz

Spatial Frequency (cyc/mm)	Modulation	Power	Spatial Frequency (cyc/mm)	Modulation	Power
0.20	0.0065	0.4077	5.20	0.0003	0.0199
0.40	0.0054	0.3403	5.40	0.0002	0.0102
0.60	0.0026	0.1613	5.60	0.0001	0.0043
0.80	0.0037	0.2326	5.80	0.0003	0.0199
1.00	0.0010	0.0605	6.00	0.0002	0.0142
1.20	0.0006	0.0358	6.20	0.0001	0.0050
1.40	0.0017	0.1079	6.40	0.0002	0.0140
1.60	0.0008	0.0490	6.60	0.0002	0.0127
1.80	0.0015	0.0961	6.80	0.0004	0.0280
2.00	0.0008	0.0472	7.00	0.0001	0.0080
2.20	0.0007	0.0470	7.20	0.0003	0.0195
2.40	0.0006	0.0351	7.40	0.0002	0.0120
2.60	0.0005	0.0302	7.60	0.0001	0.0034
2.80	0.0002	0.0118	7.80	0.0002	0.0123
3.00	0.0005	0.0291	8.00	0.0002	0.0099
3.20	0.0002	0.0133	8.20	0.0002	0.0107
3.40	0.0003	0.0168	8.40	0.0000	0.0030
3.60	0.0003	0.0210	8.60	0.0001	0.0075
3.80	0.0006	0.0352	8.80	0.0001	0.0070
4.00	0.0001	0.0035	9.00	0.0002	0.0148
4.20	0.0002	0.0106	9.20	0.0001	0.0066
4.40	0.0001	0.0064	9.40	0.0000	0.0024
4.60	0.0002	0.0100	9.60	0.0001	0.0064
4.80	0.0004	0.0247	9.80	0.0001	0.0057
5.00	0.0001	0.0072	10.00	0.0002	0.0145

Table 24. MODULATION AND POWER AS A FUNCTION OF SPATIAL FREQUENCY: 300 mV, 20 Hz – 2.5 MHz

Spatial Frequency (cyc/mm)	Modulation	Power	–	Spatial Frequency (cyc/mm)	Modulation	Power
0.20	0.0030	0.1775		5.20	0.0005	0.0320
0.40	0.0044	0.2590		5.40	0.0002	0.0122
0.60	0.0021	0.1259		5.60	0.0003	0.0187
0.80	0.0037	0.2216		5.80	0.0007	0.0391
1.00	0.0017	0.0984		6.00	0.0003	0.0162
1.20	0.0022	0.1227		6.20	0.0001	0.0081
1.40	0.0018	0.1078		6.40	0.0001	0.0072
1.60	0.0003	0.0176		6.60	0.0001	0.0033
1.80	0.0005	0.0317		6.80	0.0002	0.0092
2.00	0.0008	0.0472		7.00	0.0001	0.0030
2.20	0.0005	0.0277		7.20	0.0001	0.0063
2.40	0.0008	0.0469		7.40	0.0001	0.0068
2.60	0.0004	0.0236		7.60	0.0004	0.0209
2.80	0.0005	0.0268		7.80	0.0002	0.0135
3.00	0.0004	0.0209		8.00	0.0004	0.0268
3.20	0.0006	0.0383		8.20	0.0003	0.0157
3.40	0.0004	0.0263		8.40	0.0002	0.0138
3.60	0.0002	0.0098		8.60	0.0004	0.0233
3.80	0.0002	0.0138		8.80	0.0002	0.0131
4.00	0.0006	0.0353		9.00	0.0002	0.0115
4.20	0.0004	0.0213		9.20	0.0002	0.0103
4.40	0.0002	0.0115		9.40	0.0002	0.0122
4.60	0.0003	0.0168		9.60	0.0002	0.0106
4.80	0.0007	0.0423		9.80	0.0001	0.0031
5.00	0.0003	0.0176		10.00	0.0001	0.0037

REFERENCES

Keesee, R. L. *Prediction of Modulation Detectability Thresholds for Line-Scan Displays*. AMRL-TR-76-36 (AD-A035735), Aerospace Medical Research Laboratory, Wright-Patterson Air Force Base, Ohio, 1976.

Rosell, F. A. and Willson, R. H. "Recent Psychophysical Experiments and the Display Signal-to-Noise Concept." In L. M. Biberman (Ed.), *Perception of Displayed Information*. Plenum Press, New York, 1973, 167-231.

Snyder, H. L. "Image Quality and Observer Performance." In L. M. Biberman (Ed.), *Perception of Displayed Information*. Plenum Press, New York, 1973, 87-118.

Snyder, H. L. *Visual Search and Image Quality: Final Report*. AMRL-TR-76-89 (AD-A036263), Aerospace Medical Research Laboratory, Wright-Patterson Air Force Base, Ohio, December, 1976.

Snyder, H. L., Keesee, R. L., Beamon, W. S., and Aschenbach, J. R. *Visual Search and Image Quality*. AMRL-TR-73-114 (AD-A008007), Aerospace Medical Research Laboratory, Wright-Patterson Air Force Base, Ohio, October, 1974.